This is to certify that the
thesis entitled

DESIGN AND ANALYSIS OF MULTIFUNCTIONAL MATERIAL SYSTEMS

presented by

BHUSHAN ATMARAM EKBOTE

has been accepted towards fulfillment
of the requirements for the

M.S. degree in MECHANICAL ENGINEERING

Major Professor's Signature

11/25/2006

Date

MSU is an Affirmative Action/Equal Opportunity Institution

DATE DUE	DATE DUE	DATE DUE

DESIGN AND ANALYSIS OF MULTIFUNCTIONAL MATERIAL SYSTEMS

By

BHUSHAN ATMARAM EKBOTE

A THESIS

Submitted to
Michigan State University
in partial fulfillment of the requirements
for the degree of

MASTER OF SCIENCE

Department of Mechanical Engineering

2006

ABSTRACT

DESIGN AND ANALYSIS OF MULTIFUNCTIONAL MATERIAL SYSTEMS

By

BHUSHAN ATMARAM EKBOTE

On February, 1 2003, while re-entering earth's atmosphere, the space shuttle Columbia broke off into pieces killing all the seven astronauts. One of the major causes of this fatal accident was a breach in the Thermal Protection System (TPS) causing very high rise in temperatures inside the space shuttle. This incident motivated a need to redesign current TPS, to avoid such accidents in future. First part of this thesis discusses design evolution and analysis of a proposed new TPS using self activated, multifunction material system. Different aspects such as profile design, thermal structural issues, possibility of various material combinations etc. are taken into consideration. As design phases are coupled into fluid-thermal-structural environment, *Ansys Multiphysics 9.0* is used as design and analysis tool. In the second part, we discuss about the real life transient case analysis of a meso scale heat exchanger using functionally Gradient Materials (FGM). This simulation analyzes the possibility of thermal shock and sudden rise in stresses in the system. The final part analyzes various design issues in building a cross flow meso scale heat exchanger using different models of six layered FGM system.

When you want something with all your heart, the entire universe conspires to help you achieve it.

- The Alchemist

To mom, dad and brother Vaibhav

ACKNOWLEDGMENTS

I would like to take this opportunity to thank my graduate advisor Dr. Patrick Kwon for his relentless guidance throughout my tenure at Michigan State University. His compassionate support and motivation were the driving force in my successful completion of the degree.

I would also thank my thesis committee members Dr. Andre Benard and Dr. Hyungson Ki for their valuable suggestions and timely help. I am grateful to Jim Walker of Wah Chang Institute for providing information and material sample of ZrW_2O_8 material. My regards are also due to Ramkumar Subramanian, alumnus of our manufacturing lab for his recommendations during the research of transient state for meso-scale heat exchanger. Thanks go to my colleagues: Kyunghee Park for assisting me at heat exchanger analysis and also carrying over the perspirable skin development project after my graduation; Ben Souder for implementing my design suggestions in fabrication of perspirable skin and giving me feedback; Mark Lepech for conceptually designing the first version of cross-flow heat exchanger; Jorge Olortegui-Yume for providing lots of useful tips in research planning and presentations.

This pursuit had been impossible without the inspiration and tutelage from my brother, Vaibhav. I hope I would always get this advantage of being your younger brother, no matter where I go in my future endeavors. Thanks for being just a phone call away.

TABLE OF CONTENTS

LIST OF TABLES

LIST OF FIGURES

(Images in this thesis are presented in color)

1. DEVELOPMENT OF THERMALLY ACTIVATED MATERIAL SYSTEM FOR COOLING

1.1 MOTIVATION

On the morning of February 1st, 2003, NASA's space shuttle Columbia broke off into pieces during reentry, when it was more than 200,000 feet above Texas. Due to this accident, all the seven crew members aboard were killed. A 'Columbia Accident Investigation Board' (CAIB) was formed to study the cause of this accident and subsequent improvements in the space shuttle to avoid such incidents in future [1].

Independent researchers explored the causes of this fatal accident from various aspects. Mayeaux et al [2] studied this tragedy from materials point of view exploring the use of materials in the different sections of space shuttle and its impact over the problem. Melis et al [3] used numerical simulation method in understanding the problem. The accident was caused due to the damage sustained during launch, when pieces of foam insulation fell off the main propellant tank under aerodynamic forces and struck the left wing of orbiter at the leading edge (Figure 1.1 and Figure 1.2). This impact damaged the anti-oxidizing coating of Reinforced Carbon/Carbon (RCC) composite tile (which is one of the constituents of space shuttle thermal protection system) at the leading edge of left wing. During reentry, when the Columbia approached the layers of atmosphere, due to high friction, the temperature at the outermost layer of space shuttle increased rapidly and hot gases entered the wing through the damaged area and melted the airframe. The shuttle lost its control and broke off.

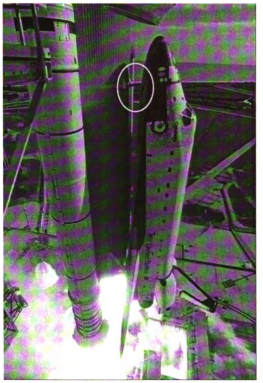

Figure 1.1: Columbia lifting off on its final mission. Circled is the Left Bipod Foam Ramp. (CAIB: Vol. I)

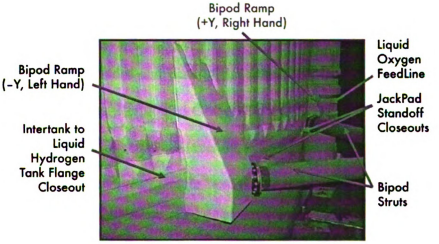

Figure 1.2: Close-up of the Left Bipod Foam Ramp that broke off and damaged the Shuttle wing. (CAIB Vol. I)

NEED FOR THERMAL PROTECTION SYSTEM

During reentry, the space shuttle orbiter is moving at about 17,000 mph (28,000 km/h), when it hits air molecules and builds up heat from friction (approximately 3000° F, or 1650° C). The orbiter's aluminum structure cannot withstand temperatures over 350° F (175° C) without structural failure. Thus, a thermal protection system (TPS) is implemented on the aluminum structure to withstand such high reentry heat.

1.2 THERMAL PROTECTION SYSTEM (TPS)

The figure 1.3 sketches TPS of an orbiter with different constituent materials. The TPS covers essentially the entire surface of orbiter with highly insulating, low conductivity material. It consists of seven different material tiles put in different locations based on amount of required heat protection. The main selection criterion for TPS is using the lightest weight protection capable of handling the heat in a given area. Sometimes, to have additional impact resistance, heavier materials are also selected.

During reentry, the front, sides and base of the orbiter are exposed to the high heat as compared to the other parts. Reinforced Carbon/Carbon (RCC) material is used to cover nose cap and wing leading edges, where reentry temperature exceeds 2300° F (1260° C). As RCC oxidizes at such high temperature, a silicon based coating is applied over it. [4]

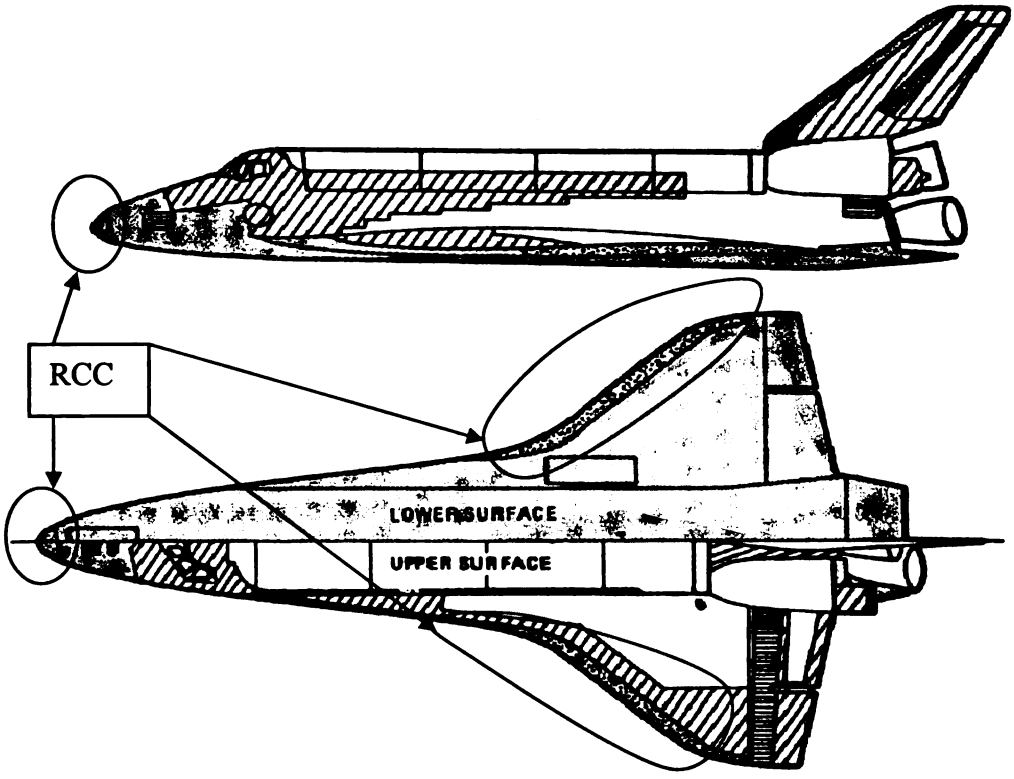

Figure 1.3: TPS materials of space shuttle orbiter

Another type of tiles used in TPS is white tiles. The white tile, made of a low-density, high-purity silica 99.8-percent amorphous fiber (derived from common sand, 1 to 2 mils thick) insulation, is made rigid by ceramic bonding. Due to the presence of up around 90 percent of void, the tile weighs only about 9 pounds per cubic foot. A slurry containing fibers mixed with water is frame-cast to form soft, porous blocks to which a colloidal silica binder solution is added. When it is sintered, a rigid block is produced that is cut and machined to the precise dimensions of individual tiles.

The main concept behind the white ceramic tile of the space shuttle is quite novel. This silica-based tile was designed to minimize the heat to transmit into the tile by reducing the thermal conductivity. Not only silica has low thermal conductivity (1.5 W/m/K at

room temperature) but also the white tile is occupied with mostly voids, which substantially lowers the thermal conductivity. Typical ceramic materials have higher thermal conductivities. However, because of the abundant voids present in the tile, the strength is sacrificed and, consequently, the tedious and cumbersome inspection after each mission is essential. On the other hand, the RCC composite tile has much higher strength. However, the RCC composites burn out when exposed to oxygen at high temperature. To prevent such oxidation, up to few millimeters of protective layers are deposited on the RCC tile. The problem with this is, once the protective layers are damaged, the tile can easily be breached due to the oxidation of RCC composites.

This motivates a need to design/improve this current TPS by using different cooling/insulating technique so as to avoid drawbacks of current protection system. Thinking of other materials, NASA has come up with a new Adaptable, Robust, Metallic, Operable, Reusable system (ARMOR) as a metallic thermal protection system [5]. Besides other problems such as low melting point (1372°C) and high density ($8.25 g/cm^3$), NASA reported that one of the main problems with ARMOR is the effect of moisture.

1.3 INTRODUCTION

The new proposed TPS design concept rectifies issues involved with current passive thermal control system by providing an actively cooled, autonomous, self-regulating multi-functional material systems which can withstand high operating temperatures and possible mechanical impacts. This new proposed system acts similar to the human skin.

Our human skin opens pores when exposed to the hotter atmosphere and spreads sweat over the skin to minimize its temperature. Similarly, with the rise in heat flux, this system opens up pores and passes cooler fluid so as bring down the temperature of surface. With lower temperatures these pores are autonomously closed providing a gap free surface. Due to its perspiring behavior, the proposed system is named as 'perspirable skin'.

This perspirable skin is a material system arranged in 'Peg and Hole' (or also called as Core and Skin) where Holes (Skin) on one material are shrink-fitted into Pegs made of another material with designed interferences between them. With Peg and Hole made of two materials with distinct Coefficients of Thermal Expansion (CTE), both of them expand differently for a given temperature, producing gap between them. This gap between Peg and Hole is opened and closed depending on the surface temperature. Cold air blow out of the gap to blanket the surface. This has proved to reduce the surface temperature substantially. With a right design, the size of the gaps is controlled so that the gap will start to open at the exactly designed temperature and the size of the gap is controlled depending on the surface temperatures. Thus, if an array of such core/skin combination is placed at the surface of space shuttle orbiter it will act as an actively cooled thermal protection system.

Using small holes to cool off the surface has been proven very effective in turbine blades application. The small holes on the blades are used to blanket the surface of the blade with colder air as the hot combustible gases are introduced into the chamber. This similar concept is carried over in this space shuttle orbiter application.

1.4 DESIGN

Figure 1.4 presents a conceptual design of core-skin arrangement of perspirable skin. Core has 4 protruding holding points (called as protrusions henceforth), which fit into similar grooves of skin holes (not shown in fig.). Further design concepts reduce this number of holding points to 2. These protruded regions hold the skin in place throughout its operation. The core and skin shown in the figure are made of two materials with distinct CTEs. The CTE of skin is larger in value than CTE of core. The skin at a relatively high temperature is shrink-fitted into the core at a room temperature. When the skin is at low operating temperatures, the gap created by the protruded regions of Core can be completely closed. At higher operating temperature, the higher CTE of the skin expands the hole (much more than Core) creating a gap between Core and Hole. Fig. 1.4 (a) and (b) only show a pair of Core and Hole in the skin. As shown in Fig. 1.4 (c), the 'Core and Hole' arrangement can be distributed throughout the skin to form an array.

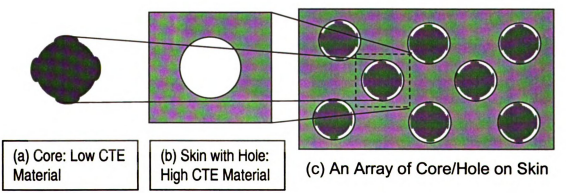

Figure 1.4: Conceptual Core-skin arrangement

This core/skin combination is designed in such way that at room temperature there is a continuous surface between core and skin with no gaps but as the temperature increases a gap starts creating between core and skin which can be later used to pass cooler air to maintain the temperature at outer surface within allowable limits.

While designing the 3D model of core/skin combination, thermal gradiency throughout the thickness of skin is taken into consideration. Figure 1.5 shows a conceptual design of 3D model. It shows the gap opening at higher temperature while protrusions and groves in contact with each other all the time. At the core base groves are created so as to allow cool airflow. A functionally designed and analyzed model will be presented in the finite element modeling part.

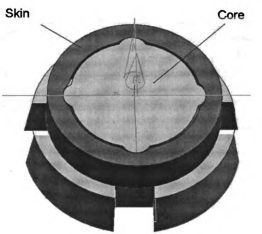

Figure 1.5: 3D Conceptual design

1.5 MATERIAL SELECTION

The area value of 'gap' at high operating temperatures is completely dictated by the physical properties of Core and skin materials. Thus core is selected from those

materials, which have very low CTE (later, NTE material is also discussed). Also, high operating temperature is another selection constraint. Materials from ceramic family are selected due to their high operating temperature and excellent compressive strength values. For the initial design and manufacturing operations mullite is used as Core, which has CTE of $3x10^{-6}$ at room temperature and reaches $6x10^{-6}$ at 1000°C. The graph below (figure 1.6) depicts the temperature dependent CTE values of different ceramics. For skin material, Zirconia (ZrO2) a high temperature ceramic with good flexural strength value is selected.

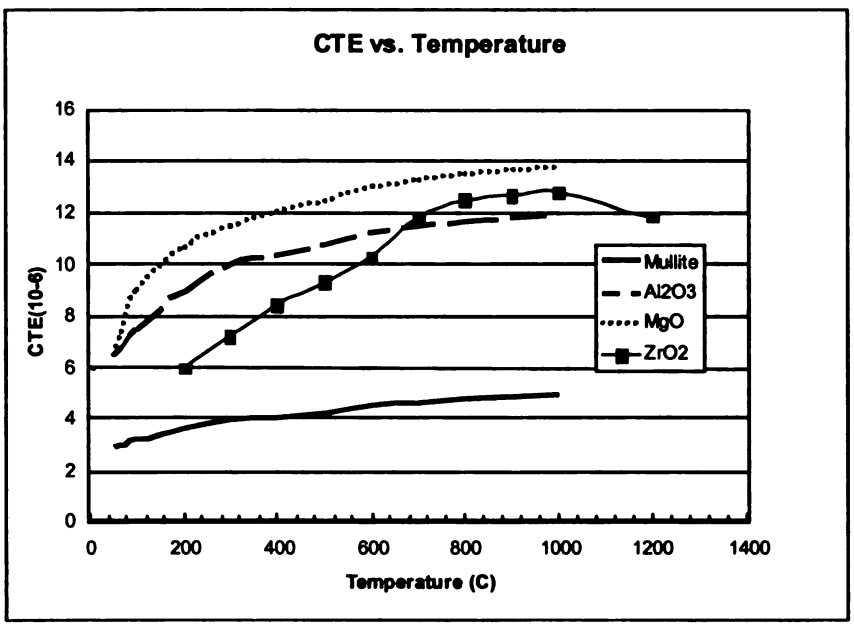

Figure 1.6: Temperature Dependency in Coefficient of Thermal Expansion [Kingery et al., 1976]

During the analysis phase, various combinations of core/skin are studies for various factors like amount of gap opening, possibility of reaction, contact stresses and resulting failure.

1.6 CONTACT DESIGN AND ANALYSIS

Figure 1.7 shows a section of Core superimposed with the contour of Hole (an arc of the circle in light solid line) in order to depict the profile of the contours. This 2-D sketch demonstrates the design parameters that will reduce the contact stress. The magnitude of the contact surface is adjusted depending on the shrink-fit pressure. With the increase in the shrink-fit pressure, the contact area will be adjusted because of the surface along α_{CN}. The contact along α_{CN} will be established to relieve the contact stresses between the protruded region and the hole.

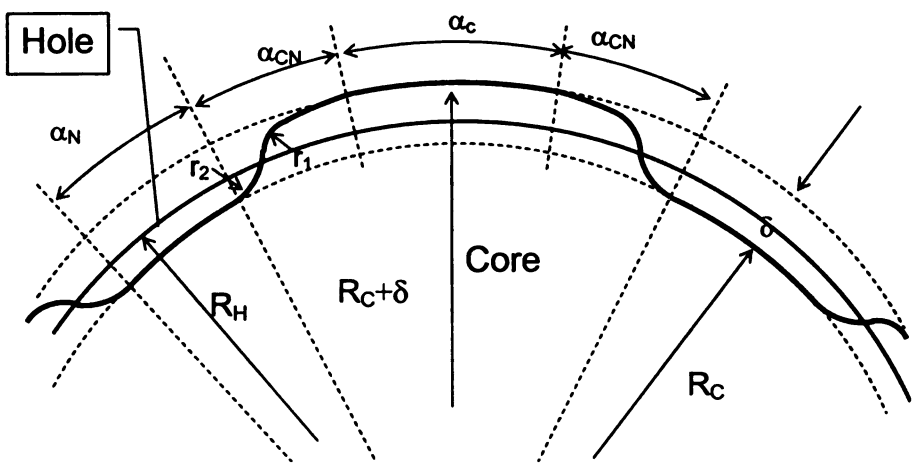

Figure 1.7: Detailed Geometric Descriptions (Contour of Core depicted in heavy solid lines and Contour of Hole depicted in light solid line)

1.7 2-D DESIGN AND ANALYSIS PHASE

As discussed above the 2-D design parameters play an important role in reducing contact stresses and determine maximum gap opening. So a design model is developed with mullite and zirconia as core and skin materials. As per our operational constraints, the protrusions of mullite should always be in contact with grooves of zirconia. Thus, we

model our shapes at a high temperature of 1800° C. Figure 1.8 shows the 2D design model. Due to the symmetry only quarter of the portion is being analyzed. Major design parameters are: diameter of mullite (core), protrusion radius of mullite, upper and lower bid fillet radii for mullite, inner diameter (ID) and outer diameter (OD) of zirconia, groove radius, upper and lower fillet radii of grooves. Considering 25° C as room temperature value, the high temperature radii for this design are calculated using simple thermal expansion equation:

$$R_{NEW} = R_{OLD}(1 + \alpha\Delta T)$$

Where:

R_{NEW} = New radius at the elevated temperature

R_{OLD} = Original Radius at start temperature

α = Temperature Coefficient of Thermal Expansion (CTE)

ΔT = Change in temperature

Designing protrusion and grooves was a major task as they are influenced by many factors. Bigger the size of protrusions will distribute the pressure thus reducing stress, but at the same time the gap opening has to be compensated as it will take the effective gap area.

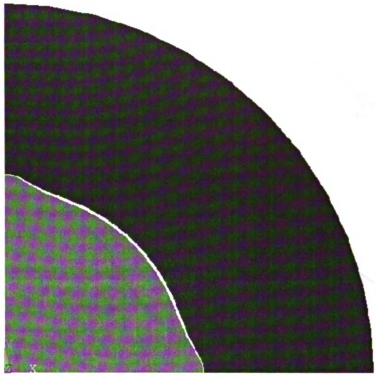

Figure 1.8: 2-D Design of core skin combination for mullite/zirconia

The protrusion height should also be designed for optimum contact, as more the protrusion height more the possibility of gap presence between mullite and zirconia contact points. Another aspect of protrusion/groove design is their gradual variation of contours. More gradual is the contour; lesser are the tensile stresses. The protrusion can also be of different shapes. Keeping the protrusion shape circular [fig. 1.9 (a)] was an advisable option not only from manufacturing point of view, but also it was providing the smooth contours. Designs were also made and analyzed for other different shapes viz. elliptical [fig. 1.9 (b)] (with larger axis along the circumference of mullite), rectangular [fig. 1.9 (c)] and diamond [fig. 1.9 (d)] shapes.

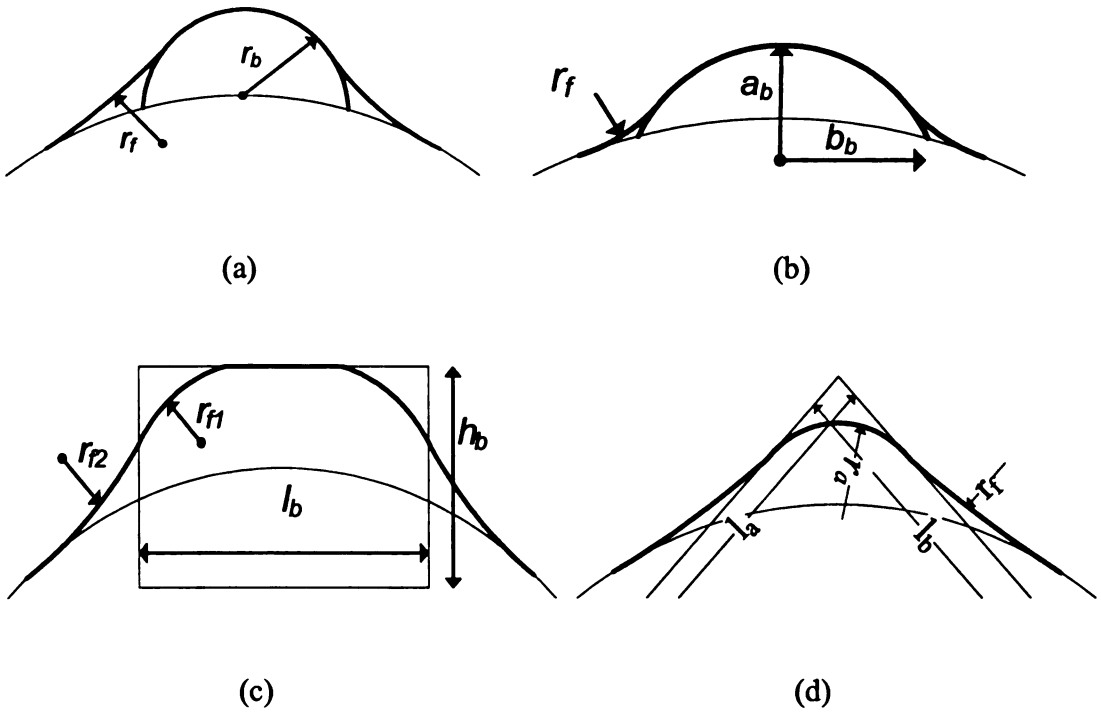

Figure 1.9: Various protrusion shape designs

Along with shapes, protrusion design involves working with various parameters like fillet radius, offset distance of center of circle from circumference of core (in circular protrusions); major minor axis values for ellipse and their center offset, location and dimension of rectangular and diamond shape protrusion, 2 different fillet radii. As per the gradual profile change requirement, circular and elliptical protrusions with larger filler radii give fewer tensile stresses without affecting the gap opening. While rectangular protrusions give more holding area they also reduce the gap opening. Due to the increase in holding area and gradual selection of fillets, stresses (both compressive and tensile) are lesser in rectangular protrusions compared with circular ones. Elliptical protrusions with horizontal major axis serve as good contact closers. So all these design models are

created and analyzed with Ansys structural analysis module and an optimum design selection is made from above different combinations.

Protrusion/groove design goes hand in hand with a major part of groove in contact with protrusion. Dimensions of fillet radii for groove become another major design parameter. Important consideration factors are 100% contact closure and minimal stress concentration points.

1.8 FINITE ELEMENT MODEL

A finite element model of a quarter shape of symmetry is chosen for analysis. 2-D shell elements with 5mm thickness are selected. The contact regions are determined and surface-to-surface deformable contact elements are selected. While defining a contact region, a contact pair needs to be identified via contact and target elements (Ansys terminology to define master and slave elements respectively). These elements will later track the kinematics of the deformation process. Target and contact elements that make up a contact pair associate with each other via a shared real constant set.

Asymmetric contact, also called as one-pass contact is defined for this analysis as we have all the contact elements on one surface and all target elements on other. Also the mesh generated is well refined and of good quality, that motivates us to use asymmetric contact. As per the selection guidelines [6], target surface is assigned to the outer (skin) concave boundary elements of zirconia. Core boundary elements are configured as contact elements. Various real constant scaling factors viz. normal contact stiffness factor, element thickness factor, and initial closure factor along with maximum contact

friction value are defined. The default Augmented Lagrangian contact algorithm is chosen. This algorithm is an iterative series of penalty updates to find exact Lagrangian multipliers (i.e. contact tractions). While choosing a friction model for this analysis, a rough contact is selected due to the possibility of dominating friction between surfaces. Also, a maximum equivalent shear stress value is set to $\sigma 1/\text{sqrt}(3)$, where $\sigma 1$ is maximum allowable principal stress for this model. A time step control option is selected so that it will predict a reasonable increment for the next sub step. Automatic time stepping is turned ON to set an accurate time step size. To avoid slow convergence rate and use of updated stiffness matrix, the Newton-Raphson option is set to FULL. Further non-linearity is added by setting Large Displacement option ON. To stabilize the calculations for large increments, the line search option is used.

1.9 PROBLEM STATEMENT

This problem is solved using two load steps. First load step works on room temperature contact/stress analysis and later one solves the model and gives the stresses and gap opening at a higher operating temperature (1500° C).

A simple static structural analysis is carried on for both of the steps. For both of the materials, the average values of Elastic Modulus (E), Poisson's Ratio (ν) and CTE (α) are provided. Symmetric boundary condition is specified at the sides of quarter circle and center of quarter circle is constrained in all directions. For step1, initial temperature is mentioned as 1800° C as our model is sketched considering the dimensions at that

temperature. A temperature load of 25° C is applied on all the nodes as the final temperature for step 1. For step 2, initial temperature is 25° C and temperature load applied is 1500° C keeping all the other parameters constant.

Numerous iterations are required for different modifications of protrusion and groove shapes. With each modification the model is optimized for the shapes. Thus, we followed the experimental simulation method for optimization.

1.10 RESULTS FOR 2-D ANALYSIS

Figure 1.10 shows contact stresses at room temperature for a circular protrusion/groove model.

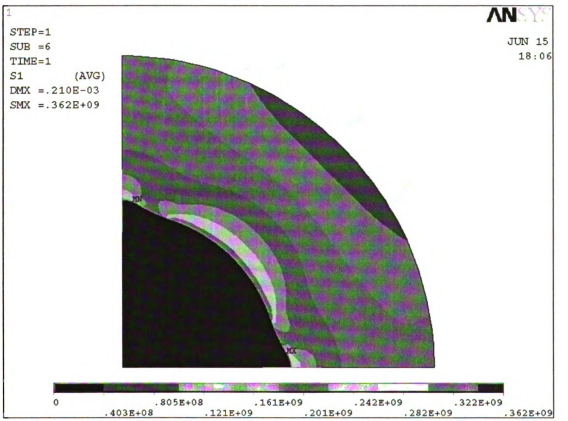

Figure 1.10: Max. Principal stresses at room temperature

This stress value (362 MPa) lies below flexural strength value for zirconia (800 MPa). This analysis also shows complete contact closure between core and skin at room temperature.

Another figure 1.11 shows minimum principal strength values at room temperature load step. These compressive stress values also look good. Fig. 1.12 shows high temperature (1500° C) maximum principal stress values. As it can be seen, the high temperature stresses in the model are lower than room temperature stresses.

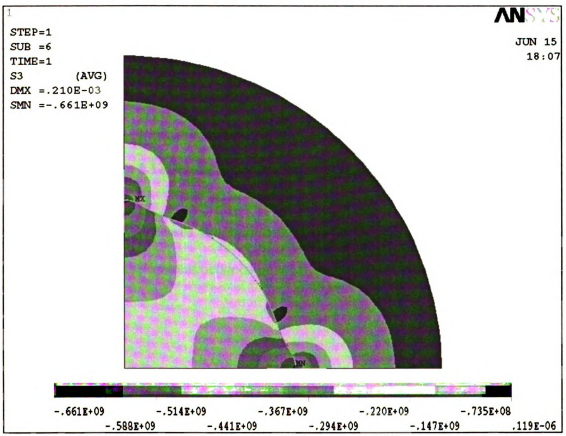

Figure 1.11: Min. Principal stresses at room temperature

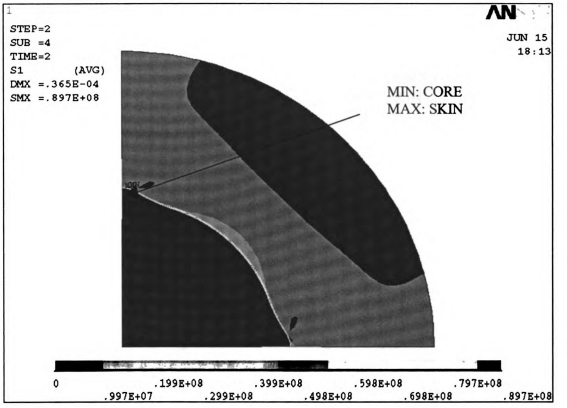

Figure 1.12: Max. Principal stresses at high temperature

Thus as temperature increases the model releases its stress. Also for the 2nd load step value, a small gap development between core and skin is seen. This gap is later utilized to pass cooler air out.

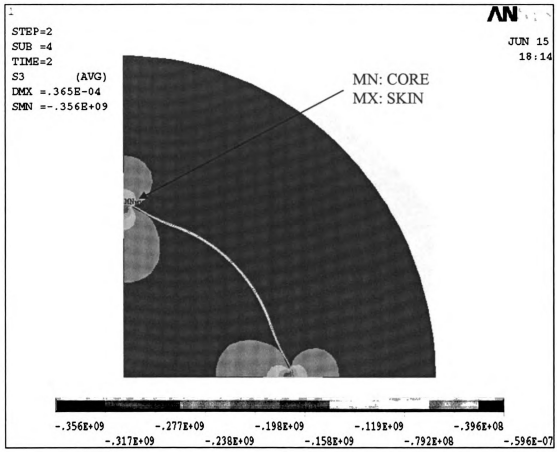

Figure 1.13: Min. Principal stresses at high temperature

Similarly, figure 1.13 shows the minimum principal stresses (compressive stresses) at high temperature value. The protrusion areas undergo a high compression over the temperature change.

Figure 1.14 show the contact status plot with 100% contact getting developed between core and skin at room temperature.

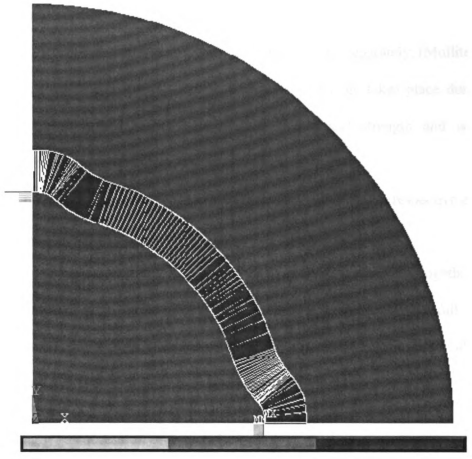

Figure 1.14: Contact status at room temperature

1.11 FABRICATION OF CORE/SKIN UNIT [7]

Mullite and Zirconia are used as core and skin respective while fabricating shrink fit (called as 2D fabrication as it involves contact profiles but doesn't cater thickness profiles of the unit). Due to the large shrinkage in ceramics during the sintering process, the machining dimensions are adjusted so as to produce right dimension assembly at the end of the process. Following are the steps that the ceramics go through in fabrication process:

1. Powder forms of mullite and zirconia are die pressed to make into discs. (force applied: mullite: 500 lb, zirconia: 3000 lb)
2. These discs are presintered in a high temperature oven separately. (Mullite: 1200° C, 2 hrs; zirconia: 900° C 2 hrs). Negligible shrinkage takes place during this process. Pre-sintered discs gain a good mechanical strength and withstand machining.
3. The profiles designed for core and skin are then machined on respective ceramics keeping in mind of possible shrinkage.
4. The pre-sintered and machined core and skin are now held together in an orientation of matching profiles. This assembled structure undergoes full sintering (T = 1475° C for 4 hr.). During this process, zirconia shrinks up to 24% while mullite up to 10% thus forming a good shrink fit assembly.

Figure 1.15 shows a successfully fabricated assembly.

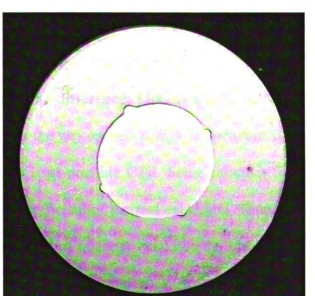

Figure 1.15: Successful fabrication using mullite and zirconia

1.12 CORE/SKIN MATERIAL COMBINATIONS

Even though as an initial prototype mullite and zirconia is selected for core and skin respectively; further research is extended in choosing right material for core as well as skin. Selection of material plays an important factor for determining efficiency of perspirable skin. Few important factors are:

- **Density of materials:** Many newer materials are being tested to make the TPS as lightweight as possible. Most of current tile material is silica filled with 90% voids. This substantially reduces the density of TPS, but at the same time makes it so fragile that one could crush a TPS tile by hand. Thus to avoid future accidents of TPS rupture due to impact, a compromise needs to be done on the density/strength parameters.
- **Maximum Operating Temperature:** As the maximum reentry temperature of the space shuttle surface can go up to 1500° C, the materials are selected which can withstand such high temperature. Ceramics, thus, become a good choice because of their high operating temperature.
- **Relative CTE value difference:** More is a CTE value difference between core and skin, more is the gap opened at high temperature. Thus for core, we need a material that has least possible CTE. Some ceramics like Zirconium Tungstate shows negative coefficient of thermal expansion. Thus, they tend to shrink when heated up. Such kind of material would be the ideal fit for core material. Some composite materials are tailored so to have CTE values as low as 0. These

materials can also be the second best option. For skin, materials having high CTE are a good fit.

- **Flexural strength values:** As the operation of skin involves contact stresses as well as thermal stresses, flexural strength of the selected material should be sufficient to bear thermal and structural loads. Ceramics generally are efficient at compressive loads but they fail poorly against bending and tensile loads.
- **Maximum principal stress produced by the combination:** This value again points towards flexural strength value and can determine the failure criteria of model.
- **Diffusing property and temperature of material:** Some metals diffuse themselves at higher temperature. Thus a ceramic/metal core/skin combination can have diffusion problems.
- **Oxidation resistance (for metals and alloys):** Metals and most of the alloys oxidize at a high temperature. Thus they might require ceramic coatings.
- **Manufacturability of materials:** Some composite materials prove to be good fit for core due to their zero CTE property, but at the same time they prove difficult to be for small fillets and accurate machining.
- **Ability of impact resistance:** Due to Columbia space shuttle disaster, the impact resistance factor is being a subject of concern. The current TPS is made of fragile silica material (which is light weight and good thermal resistant), but it proves dangerous to impacts and collisions. So considering possibility of future impacts and collisions, a material with high strength is required to be selected.

Following is the list of few metals and ceramics that are considered for either core or skin. Table 1.1 also shows some of the major physical properties.

Metal Alloys	Density (g/cc)	Yield Strength (MPa)	Max Operating Temp (C)	CTE (microns)
Fe:73 Al: 5.3 Cr:22	7.15	550	1400	15
Fe: 73 Cr:22 Al: 4.8	7.25	550	1300	15
Ni: 67.5 Cr: 30	8.14	550	1260	15
Ni: 47.5 Cr: 21.8, Fe:18.5	8.22	345	1200	16.7
Ti-3Al-2.5V	4.38	830	600	9
Ni: 80 Cr: 20	8.30	450	1200	18

Table 1.1: Metal Alloys considered for skin material

These high temperature material alloys can prove as best possible option for skin material. They have high CTE values and better yield strength. They also have good impact resistance. One drawback is high density. Using this material will make space shuttle much heavier.

Another table below (table 1.2) mentions list of few potential ceramic materials that can be used either as core or skin. (Also see Appendix A for physical properties of some common ceramics.)

Ceramics	Density (g/cc)	Compressive Strength (MPa)	Max Operating Temp (C)	Avg CTE (microns)
HfB_2–SiC	9.40	420	1800	6.5
Si3N4	2.50	550	1900	3.2
Mullite	3.16	1310	1650	5.4
Zirconium Tungstate	5.10	700	1200	-4.9
C/C Composite (w/ silicon coating)	1.50	650	1650	1.4
FSZ	6.02	2000	1800	10

Table 1.2: Ceramics considered for core/skin material

Si3N4 gives low CTE, high maximum operating temperature value as well as low density. So, if the maximum compressive stress generated using Si3N4 as core material is within limit; it can prove as a suitable fit for core material. Where as, FSZ (fully stabilized zirconia) can be a suitable match for skin material as it has high strength, high maximum operating temperature value and high CTE value. A major disadvantage using FSZ as skin is its high density.

Carbon/carbon composite, having low density and high thermal resistant properties is used as one of the tile materials in current protection system. It experiences oxidation at 800° C. Hence it's been coated with silica to increase its operating temperature up to 1600° C.

1.13 NTE MATERIALS

Out of the above ceramic materials, Zirconium Tungstate has negative CTE (hence called as NTE). This will prove as the best match for core, as when it is exposed to the high re-

entry temperature, the skin (having positive CTE) will expand and core will contract, thus creating a maximum possible gap.

Various materials having NTE are studied. Table 1.3 shows a list of few potential ceramics:

Ceramics	Avg. CTE (microns)	Temperature Range
SiO2 (faujasite)	-4.2	(25 to 573 K)
PbTiO3	-3.5	(70 - 570K)
ZrW2O8	-4.9	(0.3 - 1500 K)
AlPO4-17	-11.7	(18–300 K)
ZrV2O7	-0.25	< 1000 K
HfW2O8	-3.2	(0.3 - 1050 K)
Y2W3O12	−6.58	(473–1173 K)
Er2W3O12	−6.74	(473–1073 K)
Yb2W3O12	−6.38	(473–1073 K)
Lu2W3O12	−6.18	(473–1073 K)
Sc2W3O12	−2.2	(10–450 K)

Table 1.3: NTE Materials

Many ceramics listed above have higher NTE values than Zirconium Tungstate (ZrW2O8), but they either get decomposed or diffused at elevated temperatures. If experimental results prove that proposed thermal protection system is able to maintain lower temperature of cool air envelop, these other high NTE materials can be thought as effective and applicable. Zirconium Tungstate can be operated up to 1200° C and has considerable NTE value. So it can be safely considered as one of the possible choices for core material.

Considering the selection parameters and various mentioned material properties, few material combinations are selected and a finite element model is generated for 2D core/skin combinations. Table 1.4 shows the analysis results of these material combinations and does a comparative study about the amount of gap created by each of the combination and corresponding stresses.

Core	Skin	Core Area (m2)	Gap Area (m2)	Gap % of Core Area	Max. Principal Stress (MPa)	Min. Principal Stress (MPa)
Mullite	FSZ	7.85E-05	1.57E-06	2.00%	362	-661
Mullite	MgO	7.85E-05	2.20E-06	2.80%	195	-530
Zirconium Tungstate	MgO	7.85E-05	4.87E-06	6.20%	412	-279
C/C Composite	FSZ	7.85E-05	2.35E-06	2.99%	738	-226
Zirconium Tungstate	C/C Composite	7.85E-05	1.25E-06	1.59%	369	-500
Zirconium Tungstate	Fe-Cr Alloy	7.85E-05	5.12E-06	6.52%	385	-348

Table 1.4: Gap opening Results for various core/skin combinations

It should be noted that maximum and minimum stress values are taken from 1st load step analysis, which shows room temperature results. These values are at their maximum limits at room temperature. The gap area calculation is done after 2nd load step analysis, which displays high temperature results.

Thus, choosing particular core/skin combination can generate a gap of maximum 6.5% of core area. This much gap is substantial for passing out cooler air. Each model is required

to be optimized to ensure perfect room temperature contact between core and skin and also lowest possible stress values at room temperature.

Amongst these materials, MgO (high CTE material) has very low value for flexural strength (85 MPa), so the results predict failure of model while using MgO ceramic.

While using zirconium tungstate for core, the groove and protrusion profiles are reversed. Result contours shown below in figure 1.16 display room temperature result profiles when using zirconium tungstate as core and Fe-Cr alloy as skin.

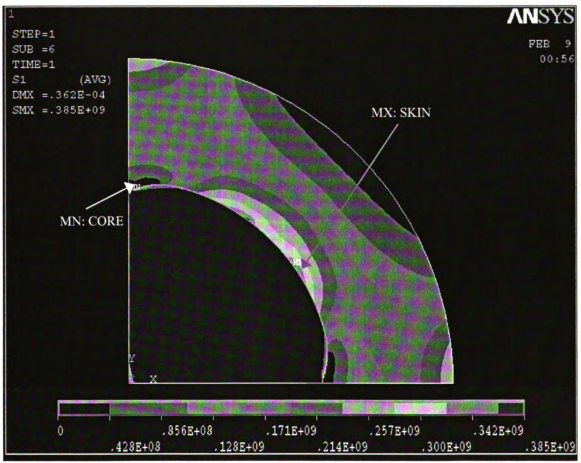

Figure 1.16: Max principal stress at room temperature for Zirconium Tungstate/Fe-Cr Alloy core/skin combination

Figure 1.17 shows compressive stress contours for the same combination.

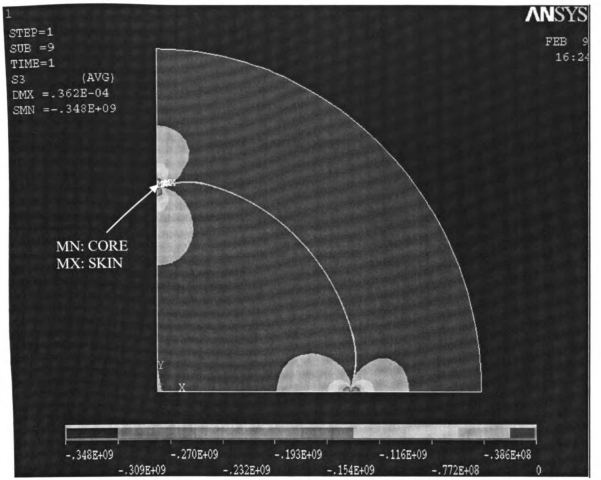

Figure 1.17: Min. principal stress at room temperature for Zirconium Tungstate/Fe-Cr Alloy core/skin combination

1.14 3D DESIGN APPROACH

The 2D design generated above is used as a top surface while generating 3D design. The important parameters to be considered are thermal gradiency, holding pressure of core to the skin at all temperatures and orientation of core towards symmetrical, unsymmetrical and curved positioning.

Due to the specific arrangement of skin/core, the temperature away from the exposed surface can drop substantially. This will cause top surface of the thickness to expand more than the bottom one. This might cause a problem in uniform opening of gap throughout the thickness. In order to compensate for this lower interior temperature, the tapered groove is designed (Fig. 1.18 (a)). This will ensure that the passage for cool air is connected throughout the operation of the perspirable skin. Fig. 1.18 (b) shows an alternative design to control the flow direction of the cooling air. In the advanced design stage, groove can be introduced spirally around Core or Hole to direct the coolant flow. Around the curved surface of the shuttle, the direction of the core can be directed to 'blow' the cool air into certain directions as shown in Fig. 1.18 (c).

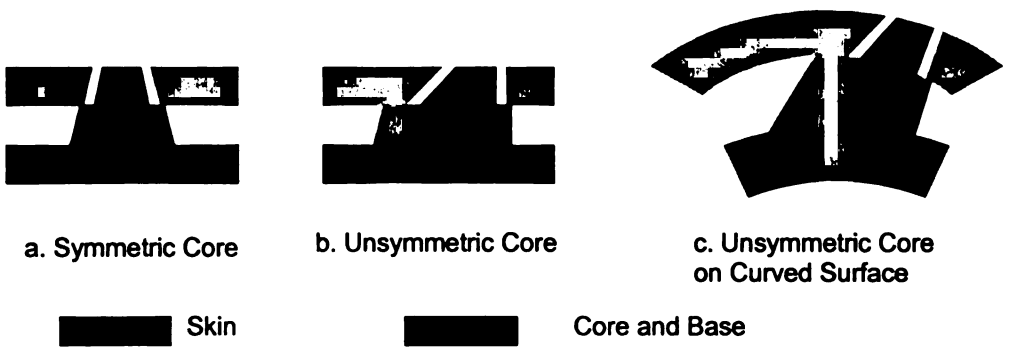

Figure 1.18: Designs to Control the Flow Direction of the Cooling Air

The skin has higher conductivity and thus it expands more than Core. Thus, the protruded regions of core and grooves are so designed that the holding pressure between them always remains substantial.

1.15 FINITE ELEMENT MODELS

Different 3D models are considered for finite element analysis. The procedure for 3D analysis follows similar structure of 2D models with an added load step. The geometry is modeled so as to mimic high temperature (1800° C higher than operating temperature) configuration. The protruded regions and grooves in contact with each other and a consistent gap developed in between. Initial geometry is designed by mathematical calculations and further modified as per simulation results.

This high temperature model undergoes structural analysis to simulate cooling to room temperature. This analysis calculates thermal stress generated due to shrinkage as well as contact stresses. A surface-to-surface contact is modeled between core and skin areas. Skin contacting surface being concave is modeled with 3D target elements and core outer surface envelopes 3D contact element. The results of this analysis are studied for gap closure and stress values. This load step gives maximum stress values; the model will carry throughout its operation, as room temperature stresses for this model setting are the maximum.

Another load step works as a parallel analysis stage, which is designed to determine temperature distribution along the thickness of model. For this, 3D coupled field (sequential) thermal elements are used. As this analysis doesn't consider cooling effect, steady state analysis will provide very high temperature values. Thus a transient thermal case is run for the finite time step till the core base temperature reaches ~200 C. This is an assumption made to simulate the temperatures contours of the model. The main

purpose of this analysis is not to determine maximum possible temperature distribution in the model, but to understand the temperature contours along model thickness.

Second load step in the structural analysis simulates a steady state heating up of model from room temperature to high temperatures. For this, the simulation starts from first load step analysis. The temperature results file from previous thermal analysis (done as a parallel analysis) is imposed as a load. Structural mounting constraints are applied. The simulation is solved for steady state structural results. These high temperature results show opening of gap and stress values. A model is considered as failure if gap is not thoroughly opened along the thickness or stresses values exceed maximum strength limit.

The model shown in figure 1.19 is one of the failed models geometry at high temperature. It has got a continuous contact between protrusion and groove, while there is a constant thickness gap between core and skin throughout the thickness. Both skin and core are modeled with a uniform taper of 10°. Skin's –z direction (vertical/along height) displacement is blocked by two legs at core base.

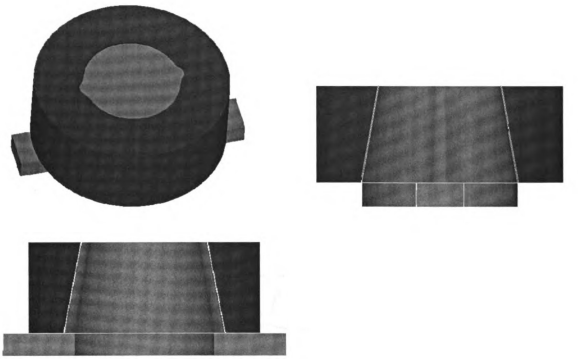

Figure 1.19: Different views of a failed model shape

This model fails in providing a continuous gap opening at high temperature. (See figure 1.20). Secondly, it also gives high principal stresses (867MPa). This can be explained as following: We have same thickness gap along the model height. At the base, due to taper, core diameter is more than that of top. The gap is calculated from top surface geometry. Thus while shrinking, bottom area shrinks more than top one and gives high stresses. In the 2^{nd} load step, while heating up, top part of the model is heated more than bottom one, as top part is exposed to the reentry heat. Thus top portion expands more than bottom. The bottom area, which is already under high shrink-fit stress, never opens up by this small temperature rise.

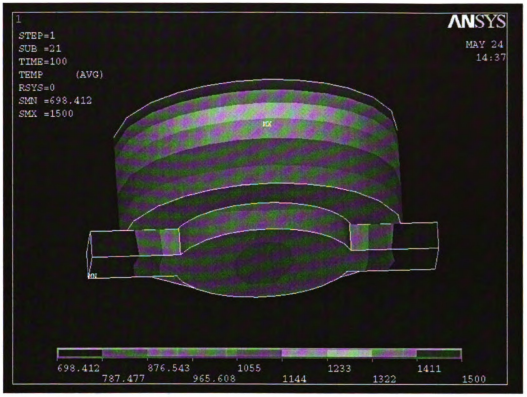
1
STEP=1
SUB =21
TIME=100
TEMP (AVG)
RSYS=0
SMN =698.412
SMX =1500
ANSYS
MAY 24
14:37
698.412
787.477
876.543
965.608
1055
1144
1233
1322
1411
1500

(a)

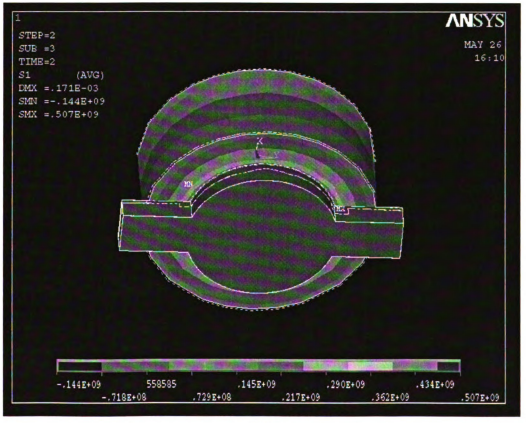
1
STEP=2
SUB =3
TIME=2
S1 (AVG)
DMX =.171E-03
SMN =-.144E+09
SMX =.507E+09
ANSYS
MAY 26
16:10
-.144E+09
-.718E+08
558585
.729E+08
.145E+09
.217E+09
.290E+09
.362E+09
.434E+09
.507E+09

(b)

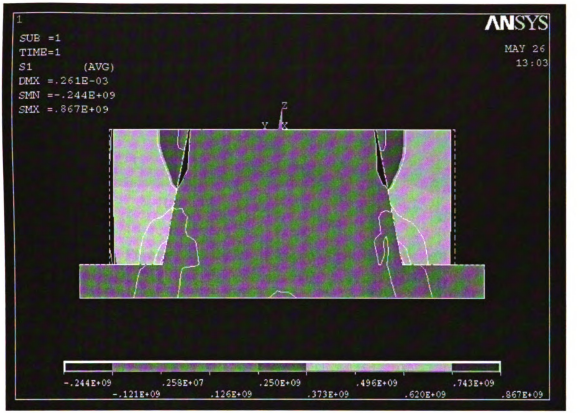

(c)

Figure 1.20: Results: a. Temperature Contours for load step 2 b. unopened gap at high temperature c. Section view of room temperature stresses

Following model shape shown in figure 1.21 tries to rectify the problems encountered in the previously discussed model.

(a) (b)

Figure 1.21: Different views of workable design

As shown, until 1mm thickness from top, both core and skin have no taper and they are in contact with one another. After this thickness, core has low taper (~1°) and the skin is designed with high taper of 10°. This creates a wide-open gap to pass the cooler air through and eliminates gap-opening problem from previous model.

This model gives satisfactory results for gap opening and room temperature stresses. One problem this model can face is its small holding area. The core and skin are gripped together through a small thickness portion (1mm). With the high velocity of coolant air or high outside pressure this holding area might prove to be insufficient and cause core dislocation.

Contour plots in figure 1.22 through 1.25 show some of the important results from analyses.

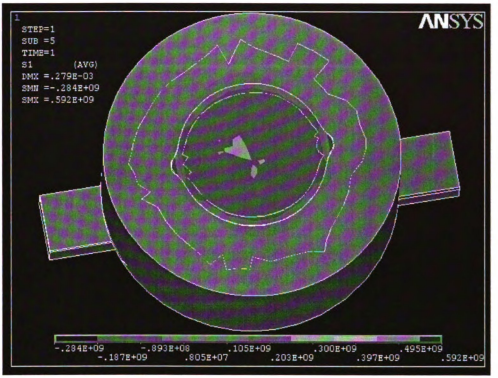

Figure 1.22: Room temperature maximum principal stresses

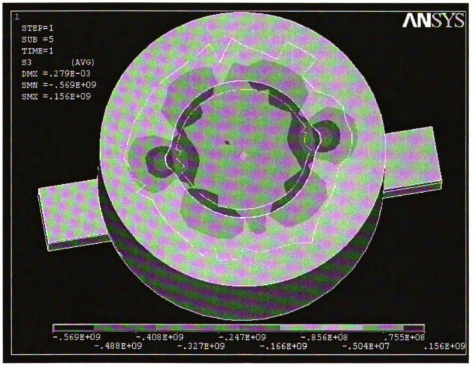

Figure 1.23: Room temperature minimum principal stresses

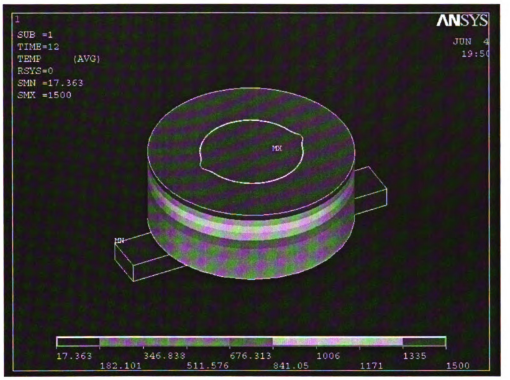

Figure 1.24: High temperature Contours

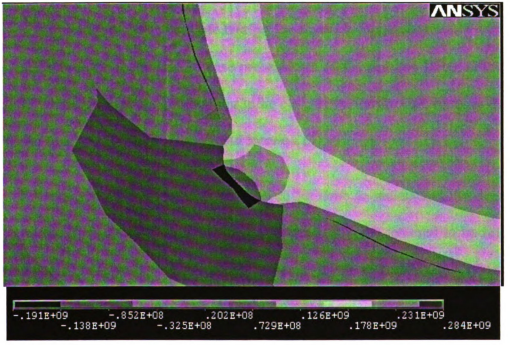

Figure 1.25: High temperature max. principal stresses

1.16 FLOW SIMULATION WITH ARRAY OF PERSPIRABLE SKIN UNITS

When the research is completed for a single system of Core and Hole on the skin, in the next step, the fabrication of series of cores and hole needs to be undertaken. By using the novel ceramic processing technique developed [8, 9, 10] the major issues like fabricating the skin and core to the exact designed dimensions and the maintaining precision in shrink-fit an array of Cores and Holes with the skin made of a single piece are overcome. Figure 1.26 shows possible design approach to fit in array of cores in the skin. Each Core can be first shrink-fitted into the skin. Subsequently, the Core based can be shrink-fitted.

Figure 1.26: Possible Design for core/skin Assembly

Figure 1.26 shows the metallic core base presented in black, ceramic Cores in gray and the skin in white. Metals are good option to be considered for the core base, as they are much easier to adjust for the alignment and location of the holes.

A model design and CFD analysis is required to be done to understand the density of cores required. Core density can be defined as number of cores required to be fitted per unit length so as to have a perfectly active cooler envelope system. To get a basic idea about the positioning and velocity required for cooler air etc., a 2D CFD analysis is done using Flotran CFD model.

1.17 CFD MODEL SETUP

Figure 1.27 shows a simple CFD model setup. As discussed above, the skin is modeled continuous and cores are shrink-fitted into it. Thick black line in the figure corresponds to skin and white rectangular areas are cores. Hot atmospheric air at 1500° C is passed over skin surface with high velocity (7500 m/s).

CFD thermo-fluid analysis is performed to generate a continuous cooler envelope over the surface by varying distance between cores and velocity of cold air passing through core.

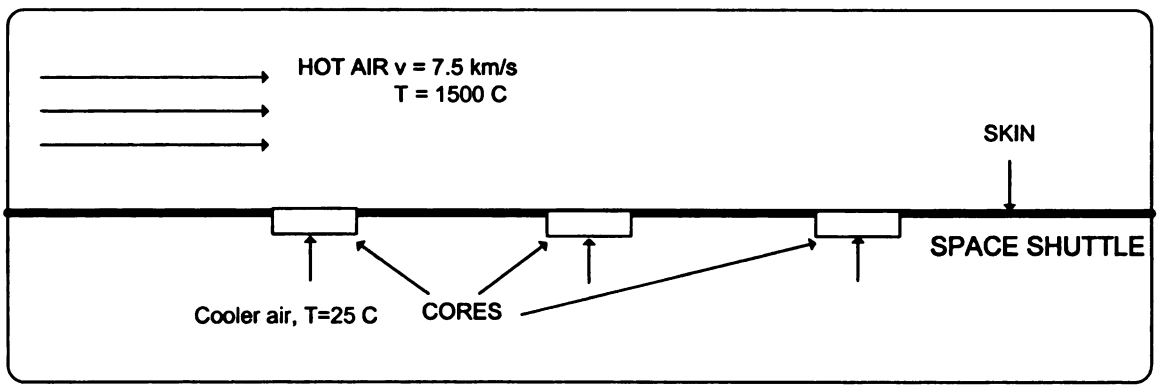

Figure 1.27: CFD model setup for flow envelope simulation

Figure 1.28 shows the result contours of this thermo-fluid analysis.

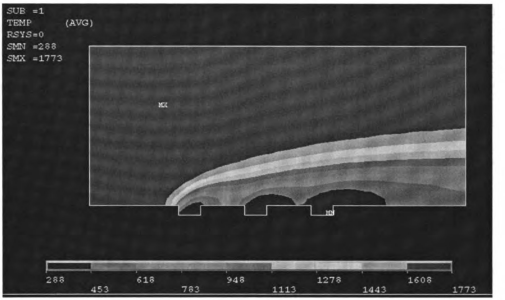

Figure 1.28: Temperature contours (K) in thermo-fluid CFD analysis

It's seen that the development of continuous envelope with average temperature of 150° C is achieved. Cores are placed 50 mm apart with coolant velocity of 75 m/s.

Though this analysis shows a basic core arrangement and gives a coarse idea of feasibility of such design, a detailed 3D analysis is required to study the behavior of arrays with thermal/fluid loading effects. Possibility of passing a liquefied cooling fluid will further change array dimensions and required coolant velocity.

1.18 SUMMARY

In this research we dealt with many aspects of the new cooling system. We successfully designed and fabricated the 2D version of 'perspirable skin' using mullite as core and zirconia as skin. We also performed the finite element analysis (FEA) for this model and

the results showed permissible stresses in the model at all the operating temperatures. A research on the range of different material combinations for core and skin is also done and their relative advantages and disadvantages are studied. For that, some negative CTE materials are also studied. It is seen that with zirconium tungstate (an NTE material) core and Fe-Cr alloy skin, the model develops larger gap amongst the combinations. Later 3D model is also designed and analyzed for different shapes and were studied for relatives stresses. A successful 3D model is generated which will perform satisfactorily at all working temperatures. From the fluids' dimension, a CFD analysis is done to understand how the model will look like after it's assembled in the space shuttle outer layer and how efficient it will be with the high heat flux exposure. The model is proved to be performing as per expectations under hot fluid temperature and high velocity.

1.19 RECOMMENDATIONS FOR FUTURE WORK

This project is still under research and development phase. More refinement in the 3D model shape can be done. Spiral grooves and protrusions should be tested for better fluid performance. 3D model fabrication is another important task from manufacturing point of view. Currently most of the simulations are done considering mullite as core and fully stabilized zirconia as skin. Other low-density materials, NTE materials (viz. zirconium tungstate) and also some metal alloys need to be carefully considered for better performance. Further CFD analysis is required to be done to design the coolant air passage structure. This structure has to be optimized for best fluid flow.

Considering the application of this skin into space shuttle orbiter, the fitment of core into current space shuttle system needs to be designed. Core can be shrink-fitted into core base, which can be further glued or fixed to the aluminum body of orbiter.

Instead of air as a coolant, some other fluids should also be researched. One of the options can be liquefied gas. This will give increased flow pressure as well fasten the cooling rate. In such case the 3D perspirable skin needs to be designed to accommodate such high-pressure coolants.

2. STEADY STATE AND TRANSIENT ANALYSIS OF MESO-SCALE HEAT EXCHANGER

2.1 INTRODUCTION

As the current electronic industry aims towards miniaturization of component, the power density of such components is rapidly increasing. Heat dissipated by small electronic chip can go as high as 500 kW. This increased heat dissipation is coupled with limited heat removal surface area [11]. For such high heat flux, the conventional heat rejection techniques of conduction and forced convection are insufficient. There is a need of more efficient heat removal method which can occupy least space and remove maximum of heat energy.

Gerlach et al. [12] modeled 3D stacked chip electronics with solid heat spreaders. They found that solid heat spreaders can be used to conduct the heat from the interior of stacked chip electronics to the periphery if the heat transfer coefficient to the ambient is high enough. Some researchers have studied the development of microchannel heat sinks [13]. Joo et al. [14] developed the method of batch fabrication of monolithic microchannels for microelectronics chip cooling by building monolithic microchannels directly on the heated front surface of the IC chips by micro-electroplating. This eliminated the need to bond heat sink to the IC chip.

This topic presents a concept of actively cooled heat exchanger which can work with high heat flux removal and will be compact enough to act locally with electronic chips. This proposed heat exchanger will have an array of internal channels built in a meso scale

disk, through which a cooler fluid can be passed to remove the heat from the source. It is also designed to operate in various different heat impulse conditions. Due to an even thermal loading, it is predicted to induce thermal stresses in the body of the exchanger. To minimize these stresses, instead of homogenous materials, a Functionally Gradient Material (FGM) is used in fabrication.

An FGM consists of a layered combination of different materials with each layer having distinct material property tailored for the application requirement. Each layer can be prepared by homogenously mixing two powders in different ratios and then stacked together to form a discrete thermo-mechanical gradiency.

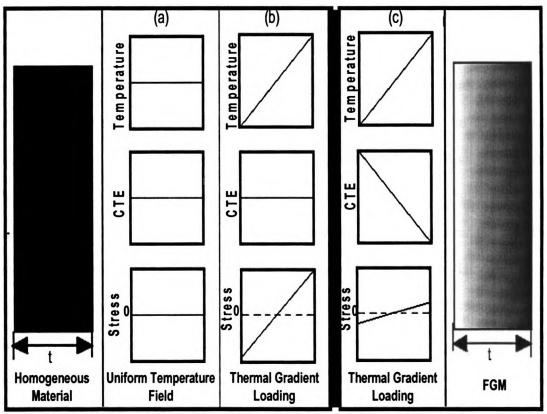

Figure 2.1: Concept of FGM

Figure 2.1 supports the idea of implementing FGM in the fabrication of such type of heat exchangers. Considering the heat exchanger as a disk attached to the packaging surface of the electronic equipment, one face of the disk is exposed to the high heat source and the remaining surfaces are at the atmospheric temperature. So, there is a thermal gradiency from one face of the disk to the opposite face. A disk made of homogenous material has constant material properties throughout the thickness. This disk when exposed to the uniform temperature at all the surfaces will produce no residual stresses in its body (Fig.2.1 (a)). But when the same disk is exposed to the thermal gradient environment as discussed for the electronic cooling application, will produce a sharp distribution of residual stresses (Fig.2.1 (b)). This is due to a constant value of Coefficient of Thermal Expansion (CTE) throughout the thickness of the disk which is responding to the uneven heating. To tackle such thermal gradient loading, FGM serves as a perfect alternative. The layer combination in FGM is selected in such a way that the layer that is exposed to the heat flux is made of low CTE material. The layers next to it are made of materials having CTE in the increasing order. Thus the thermal gradiency of the application is neutralized by the structured combination of materials with distinct CTE values. So when a disk made of such FGM is exposed to the thermal gradient loading, the resultant residual stress is minimal (Fig2.1 (c)). An ideal FGM for such application will have practically infinite layers to give a smooth change in material properties. Though, through experiments an acceptable combination of layers can be determined. This number is also chiefly governed by the manufacturability of such combination.

2.2 FABRICATION OF FGMs

A wide range of processes, such as plasma spraying, centrifugal casting, common powder metallurgy and colloidal processing have been reported for FGM production. Liu et al. [15] also fabricated functionally graded TiC/Ti composites by Laser Engineered Net Shaping. In bulk FGM fabrication, powder metallurgy is the most common processing technique. This technique was first developed by Watanabe and Kawasaki (1992) [16]. They also developed the spray deposition technique and differential temperature sintering of material species. Later various researcher developed new ideas in processing of FGMs and multilayer ceramics. Neubrand et al. [17] also compared the powder metallurgy technique of preparing FGMs with non-conventional methods such as sedimentation.

Preparing an FGM involves various challenges. In making FGMs, at least two materials with distinct properties must be mixed and processed inhomogeneously to create the gradient properties of FGMs. The fabrication processing techniques, however, have not been as well established because not only the processing depends on the choice of material combination but also the process-induced residual stress can be too intense to cause cambers and cracks in FGMs as shown in Fig. 2.2. The residual stress emanate from the difference in the coefficient of thermal expansion and the high processing temperatures. [18]

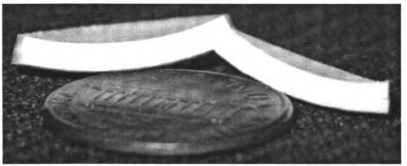

Figure 2.2: Two-layered Ceramics made of PSZ and Alumina exhibiting a Large Camber

To tackle the issue of residual stress while fabricating FGM, a novel powder processing technique is used [18]. In this, the CTE mismatch is compensated by manipulating the powder packing before sintering. Powder packing is controlled by using powders with distinct particle size and co-compacting followed by co-sintering. The different internal shape requirements such as internal channels in our model are fabricated by using fugitive phase.

2.3 MODEL SETUP

The proposed cooling technique mentioned in this topic is a meso-scale heat exchanger device which has 8 cooling channels embedded into it. This device gains multifunctionality as it can also act as a skin of electronic equipment. Due to small size and closeness to the heat dissipating area, this heat exchanger gets an advantage. Thermal gradiency is imposed due to the heat flux imposed on a single face of heat exchanger where as all other faces remain at atmospheric conditions. Due to the uneven heat

distribution along the body of heat exchanger, a large amount of thermal stresses can be generated for a homogeneous material. This effect is offset by using FGM.

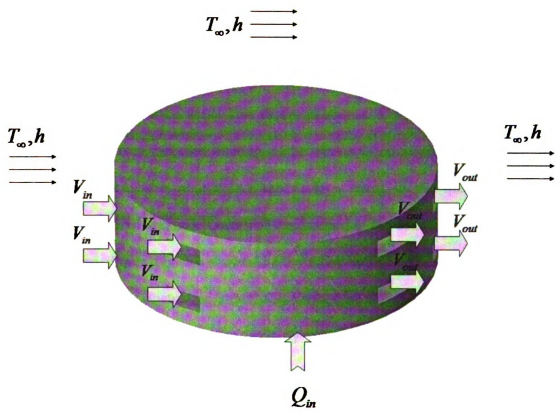

Figure 2.3: Operational view of heat exchanger

Figure 2.3 shows the proposed model. It consists of a disk shaped heat exchanger made of 3-layer equal/unequal thickness FGM with 8 cooling channels. The powders used in this FGM model were Alumina and Partially Stabilized Zirconia (PSZ), so chosen due to their interfacial strength and differences in their CTE values. To calculate mechanical properties of FGM as a function of volume fraction of particles or fibers, Mori-Tanaka (1973) approach is used [19].

2.4 MORI – TANAKA APPROACH

As our proposed model has FGM layers of the combination of alumina and zirconia, the top and bottom layers will be of pure ceramics alumina and zirconia respectively. But the layers in between are a combination of proportionate mixture of alumina and zirconia. To determine the effective material property of such inhomogeneous ceramic composites, Mori-Tanaka scheme can be used. This theory discusses "a method of calculating the average internal stress in the matrix of a material containing inclusions with transformation strain. It is shown that the average stress in the matrix is uniform throughout the material and independent of the position of the domain where the average treatment is carried out. It is also shown that the actual stress in the matrix is the average stress plus the locally fluctuating stress, the average of which vanishes in the matrix. Average elastic energy is also considered by taking into account the effects of the interaction among the inclusions and of the presence of the free boundary." [19]

As per Mori-Tanaka, the effective stiffness tensor can be expressed as [20]:

$$C^{*} = C^{MT} = C_m + v < (C_f - C_m) A^{MT} >$$

where,

v = represents the volume fraction of particles or fibers

C_m = stiffness tensor of the matrix material

C_f = stiffness tensor of the particle (fiber) material

A^{MT} = strain concentrator

Also, the effective thermal expansion coefficient (CTE) tensor α^+ is calculated using Mori-Tanaka approach as:

$$\alpha^+ = \alpha_m + (\alpha_f - \alpha_m)(S_f - S_m)^{-1}(S^{MT} - S_m)$$

In the above equation,

α_m = CTE of the matrix material

α_f = CTE of the particle material

S_m = Compliance tensor of the matrix material

S_f = Compliance tensor of the particle material

S^{MT} = The effective compliance tensor

Similarly the other effective properties of the composite are calculated as mentioned below:

For thermal conductivity:

$$K^* = K_m + v(K_f - K_m)A^{MT}$$

where,

K_m = Thermal conductivity of the matrix material

K_f = Thermal conductivity of the particle material

v = Volume fraction of particles or fibers

A^{MT} = Strain concentrator

For specific heat of the composite material:

$$C = V_m C_m + V_f C_f$$

where,

V_m = Volume fraction of the matrix phase

V_f = Volume fraction of the particle phase

C_m = Specific heat of the matrix material

C_f = Specific heat of the particle material

Also to calculate the density of material at constant temperature, the law of mixtures can be used:

$$\rho = V_m \rho_m + V_f \rho_f$$

where,

ρ_m = Specific heat of the matrix material

ρ_f = Specific heat of the particle material

The powders used in our model are alumina and partially stabilized zirconia. The six-layer FGM made from these powders will have varying proportion of combination mixtures. The effective material properties of these composites were calculated using the formulae mentioned above. Because alumina and zirconia have similar particle size, these equations were solved twice, once using alumina as matrix phase and then later having PSZ as matrix phase. The values obtained from each method were then averaged to get the final values [20].

A finite element analysis is performed on this model with imposed thermal loads as heat flux and convective boundary conditions. Also mechanical clamping constraints are applied. Comparison of maximum principal stress value was done between alumina, 3-layer FGM as well as 6-layer FGM [20]. Stresses are also compared between 3-layer equal thickness, thicker alumina layer, and thicker Zirconia layer models.

In the second part of this research we deal with a special transient analysis case for this model. Steady state analysis provides us with the final stable values of thermal stresses. But it ignores the thermal shock, which might occur at the beginning of the heat exchanger. Here we solve the FEA model of 3-layer FGM heat exchanger to analyze the stresses produced due to thermal shock of sudden cooling.

2.5 PROBLEM STATEMENT

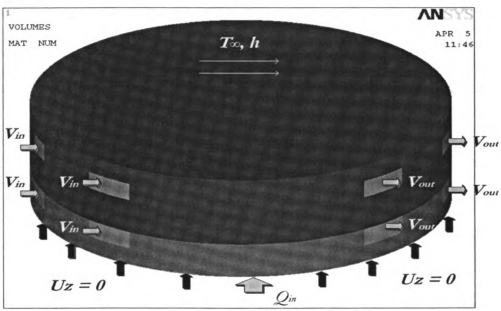

Figure 2.4: Heat Exchanger Model Setup

Figure 2.4 shows the finite element model setup. The heat exchanger disk has 8 cooling channels. Heat flux of 250kW/m^2 is imposed on the bottom surface. Water flows through the channels with inlet velocity of 0.5 m/s and initial temperature of 15° C; thus providing cooling. Atmospheric convection (h = 60 W/m^2/K, T = 25° C) is imposed on surroundings. Also bottom surface clamping constraint is taken into consideration so that the model is allowed to move in X, Y direction, but is constrained to move in Z direction (Uz=0) (Considering a co-ordinate system which has X and Y axes along the circular plan of the disk and Z axis along the thickness of the disk).

Following are geometrical parameters of the model:

Disk Diameter: 20 mm

Disk thickness: 6mm

Cooling Channels c/s: 1.6mm width x 1.0 mm height

Dist. Of channel layer above disk surface: 1mm

Center to center dist. between consecutive channels: 5 mm

Transient Case:

This special transient case analysis deals with the sudden thermal loading conditions. The step by step discussion is as mentioned below:

- Water inside the channels is stagnant at the beginning (time t=0) with temperature at 15° C.
- Heat flux of 250kW/m^2 is applied at the bottom surface (t=0) and all other faces are exposed to ambient conditions.
- Bottom surface is mechanically constrained at Uz = 0 and the center point of bottom surface is given All DOF = 0

- Analyze the increase in temperature results till temperature at the bottom channels approach 100° C. (transient thermo-fluid analysis)
- Start the water flow at this time (The time when temperature near bottom channels is near the boiling point of water).
- Analyze the stresses in the body of heat exchanger (thermo-structural analysis) for the unit time increments till the variation in stresses with respect to time zeros down. Thus the thermal shock is monitored.

The FGM used is made of three layer combination of Alumina and PSZ combination. Of the three layers, bottom-most layer; which is exposed to heat flux is made of 100% Alumina, as Alumina has lower CTE. Middle layer is a mixture of 50% Alumina and 50% Zirconia. Top layer is 100% PSZ which has higher CTE. As discussed in the previous section, the properties of this mixture ceramic are evaluated using Mori-Tanaka (1973) scheme. (See Appendix B for the essential mechanical properties.). Also, three different models of FGM are evaluated based on the thickness of each layer (Figure 2.5).

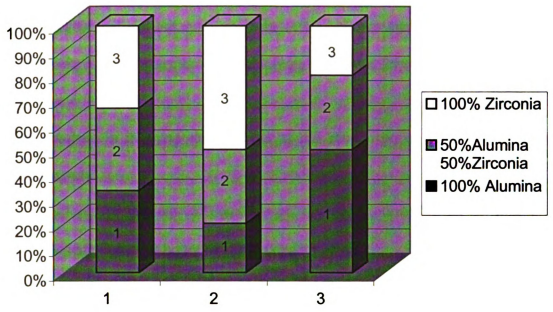

Figure 2.5: Three different models of FGM

The model where all the layers of the FGM are equally thick (Fig. 2.5.1) is considered as the baseline model. Where as the model with thinner bottom most layer (pure Alumina layer also called as Model 2 hereafter) is compared with the model with thicker bottom most layer (pure Zirconia layer also called as Model 3 or thinner zirconia layer model hereafter) and the results are compared for the least stresses.

2.6 FINITE ELEMENT MODEL

As this problem is made of two parts, the steps involved in each part are mention below:

Static thermo-fluid-mechanical analysis:

1. A steady state CFD analysis is run to calculate temperature distribution in the model due to acting heat loads and cooling channels.

2. Transferring the CFD model into structural model. Retrieving temperature results from CFD analysis and applying them as temperature loads. Other mechanical clamping constraints are also added. Solving this model for stresses.

The steps involved in transient step analysis of this model can be broken down into following subparts:

1. Performing transient CFD analysis of 'stagnant fluid model' for the time till the temperature at bottom channels reach 100° C
2. Transient CFD analysis of 'fluid flow model' done for time step T=1 sec. after stage 1
3. Solving the model for structural analysis using results of stage 2. Solving for stage 2 again for the next time increment.
4. Monitoring the results at each time step till steady state is reached.

Ansys Multiphysics was used to solve this finite element analysis problem. As this problem involved interaction of fluid (cooling water flow), thermal (Heat flux, convection B.C.) and structural (strains due to thermal changes and heat flux gradiency) analysis, the Coupled Field Analysis was implemented.

Certain aspects of the previous heat exchanger model are also tried to modify. A clamping constraint at the bottom surface is added, so as to prevent it to move in Z-direction, which is normal to the disk body; but it is allowed to move in X, Y directions, along the surface of the disk.

COUPLED FIELD ANALYSIS

Coupled-field analyses are useful for solving problems where the coupled interaction of phenomena from various disciplines of physical science is significant. In our problem we have temperature field giving rise to thermal strains and also temperature dependent material properties.

There are basically two methods of coupling distinguished by the finite element formulation techniques used to develop the matrix equations [21]. These are illustrated here with two types of degrees of freedom ($\{X_1\}$, $\{X_2\}$):

1. Strong (simultaneous, full) coupling - where the matrix equation is of the form:

$$\begin{bmatrix} [K_{11}][K_{12}] \\ [K_{21}][K_{22}] \end{bmatrix} \begin{Bmatrix} \{x_1\} \\ \{x_2\} \end{Bmatrix} = \begin{Bmatrix} \{F_1\} \\ \{F_2\} \end{Bmatrix}$$

   and coupled effect is accounted for by the presence of the off-diagonal sub-matrices $[K_{12}]$ and $[K_{21}]$. This method provides for a coupled response in the solution after one iteration.

2. Weak (sequential) coupling - where the coupling in the matrix equation is shown in the most general form:

$$\begin{bmatrix} [K_{11}(\{x_1\},\{x_2\})][0] \\ [0][K_{22}(\{x_1\},\{x_2\})] \end{bmatrix} \begin{Bmatrix} \{x_1\} \\ \{x_2\} \end{Bmatrix} = \begin{Bmatrix} \{F_1(\{x_1\},\{x_2\})\} \\ \{F_2(\{x_1\},\{x_2\})\} \end{Bmatrix}$$

and the coupled effect is accounted for in the dependency of $[K_{11}]$ and $\{F_1\}$ on $\{X_2\}$ as well as $[K_{22}]$ and $\{F_2\}$ on $\{X_1\}$. At least two iterations are required to achieve a coupled response.

For Thermal-Structural analysis of our problem we consider weak coupling.

Following are advantages and disadvantages of Coupled-Field formulation:

Advantages:

1. Allows for solutions to problems otherwise not possible with usual finite elements.
2. Simplifies modeling of coupled-field problems by permitting one element type to be used in a single analysis pass.

Disadvantages:

1. Increases wavefront (unless a segregated solver is used).
2. Inefficient matrix reformulation (if a section of a matrix associated with one phenomenon is reformed, the entire matrix will be reformed).
3. Larger storage requirements.

Following is the matrix equation for Thermal-Structural analysis:

$$\begin{bmatrix} [M] & [0] \\ [0] & [0] \end{bmatrix} \begin{Bmatrix} \{\ddot{u}\} \\ \{\ddot{T}\} \end{Bmatrix} + \begin{bmatrix} [C] & [0] \\ [0] & [C^t] \end{bmatrix} \begin{Bmatrix} \{\dot{u}\} \\ \{\dot{T}\} \end{Bmatrix} + \begin{bmatrix} [K] & [0] \\ [0] & [K^t] \end{bmatrix} \begin{Bmatrix} \{u\} \\ \{T\} \end{Bmatrix} = \begin{Bmatrix} \{F\} \\ \{Q\} \end{Bmatrix}$$

where:

$[K^t] = [K^{tb}] + [K^{tc}]$

$\{F\} = \{F^{nd}\} + \{F^{th}\} + \{F^{pr}\} + \{F^{ac}\}$

$\{Q\} = \{Q^{nd}\} + \{Q^{g}\} + \{Q^{c}\}$

and: [K] = Structural stiffness matrix; $[K^t]$ = Thermal conductivity matrix; $[K^{tb}]$ = Thermal conductivity matrix of material; $[K^{tc}]$ = Thermal conductivity matrix of convection surface;

{F}: Force Vector; $\{F^{nd}\}$: Applied nodal force vector; $\{F^{th}\}$: Thermal strain force vector; $\{F^{pr}\}$: Pressure load vector; $\{F^{ac}\}$: Force vector due to acceleration effects (i.e., gravity)

{Q}: Heat flow vector; $\{Q^{nd}\}$: Applied nodal heat flow rate vector; $\{Q^{g}\}$: Heat generation rate vector for causes other than Joule heating; $\{Q^{c}\}$: Convection surface vector

[M]: Structural mass matrix; [C]: structural damping matrix; $[C^t]$: Thermal specific heat matrix; {u}: Displacement vector; {T}: Thermal potential vector

As stated before, sequentially coupled (weak form) solving technique is used for thermal structural analysis.

PROCEDURE FOR SEQUENTIALLY COUPLED-FIELD ANALYSIS

Of the two methods of sequential analysis (indirect, physics environment), the indirect method is implemented. In indirect method, you maintain different databases and results files. Figure 2.6 shows the data flow for a typical sequential analysis done with the indirect method. Each data base contains the appropriate solid model, elements, loads, etc. You can read information from a results file into another database. Element and node numbers must be consistent between the databases and the results file.

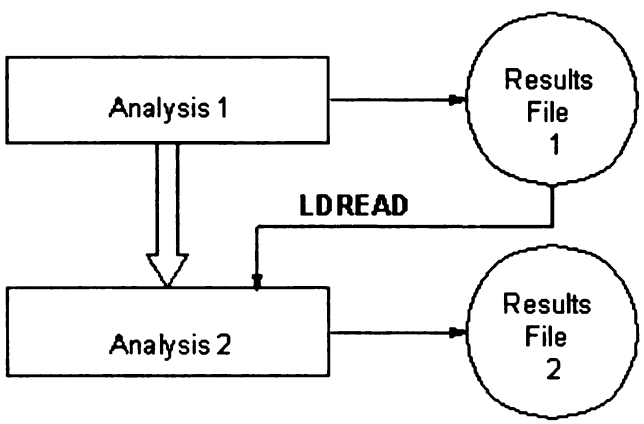

Figure 2.6: Data Flow For A Sequential Coupled-Field Analysis

For CFD analysis 3D Flotran elements were used. Once the CFD analysis is performed the result file is used as a load file for next step. Element type is changed from Flotran to 3D Structural elements. Structural constraints are then imposed and model is solved for thermal stresses. For accurate results, variations in the thermal properties of material as well as water are mentioned.

Initially, while performing steady state analysis all three, equal layer, thinner alumina layer and thinner Zirconia layer models are solved. In equal layer model, each layer is 2

mm thick. In thick Alumina layer model Alumina is 3mm thick, 50-50 is 2 mm and PSZ (TZ-3YS) is 1mm thick. In thick Zirconia model this sequence is reversed, i.e. (TZ-3YS) is 3mm thick, 50-50 2mm and Alumina 1 mm. The optimum model for given set of conditions is chosen and this model is used for the further case of transient analysis.

2.7 RESULTS AND DISCUSSION: STEADY STATE ANALYSIS

For steady state analysis, from the three models that are simulated: thinner alumina layer, thinner zirconia layer and equal thickness layer; the thinner Zirconia layer model proves to be the best. It gives minimum value for maximum principal stress amongst three. Thin alumina model gives maximum value of 285 MPa and that of equal thickness model is 213 MPa whereas 168 MPa is for thinner Zirconia model. These values are for heat flux of 250kW/m^2 and bottom clamping constraint and might vary by changing clamping condition and/or heat flux values. Figure 2.7 and 2.8 shows maximum principal stress and temperature contours for thinner Zirconia model. Figure 2.9 and 2.10 shows a comparative graph of variations in stress across thickness for all three models.

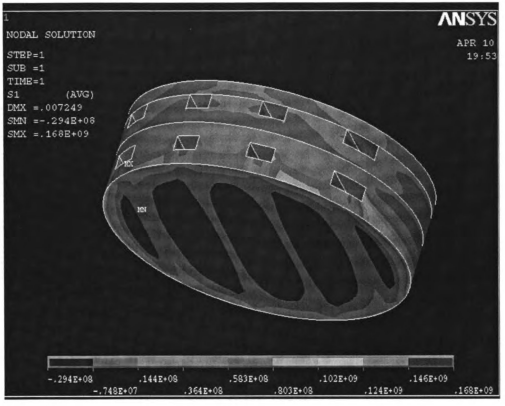

Figure 2.7: Maximum Principal Stress Contours: steady state analysis thinner Zirconia model

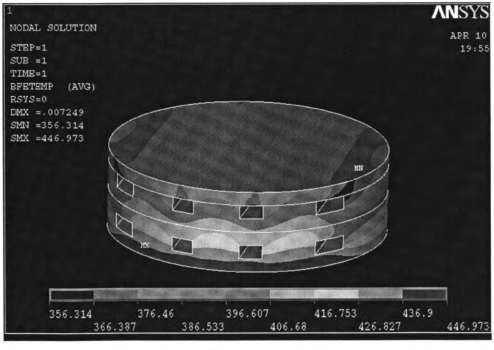

Figure 2.8: Temperature (K) Contours for steady state analysis of thinner Zirconia model

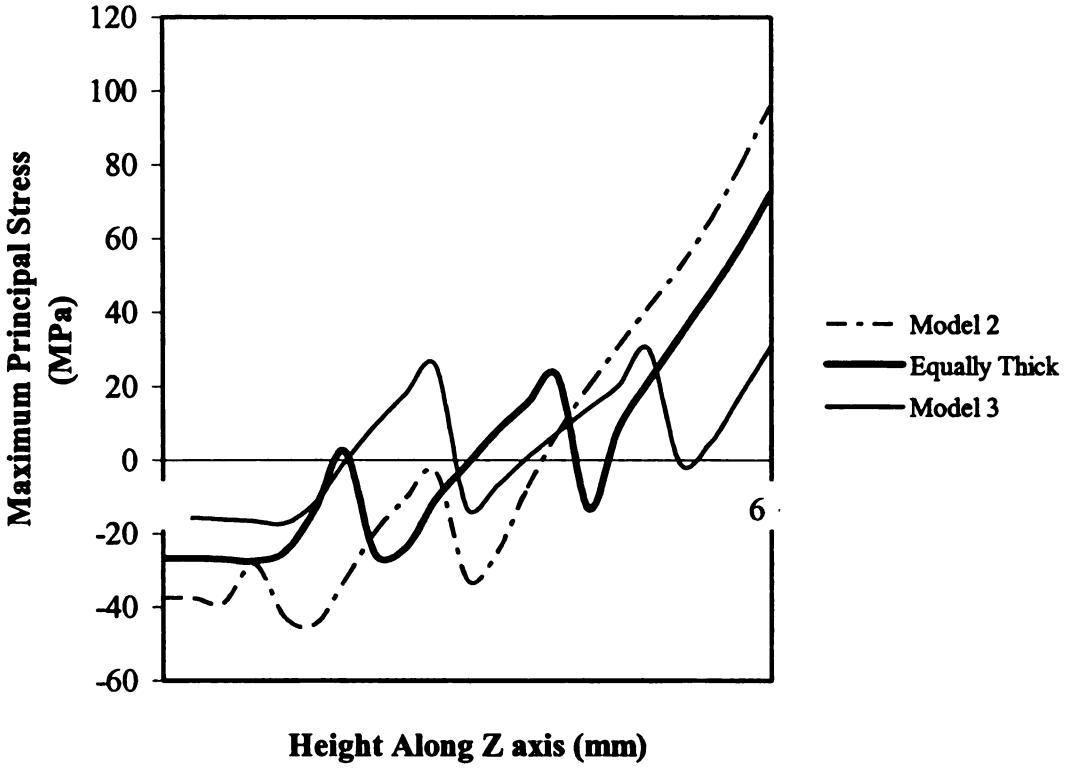

Figure 2.9: Maximum Principal Stresses for FGM model at x = 0, y = 0 mm

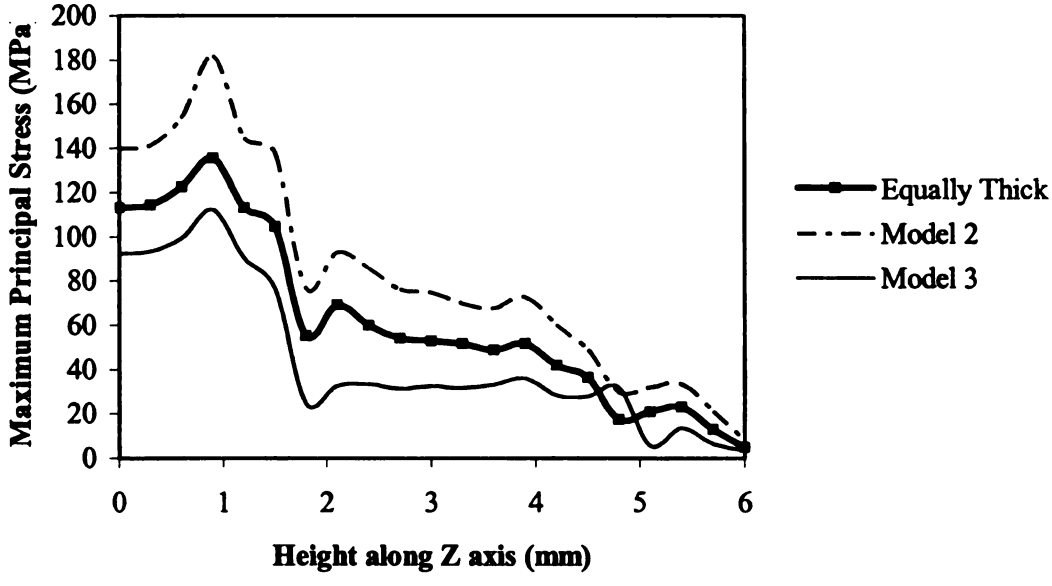

Figure 2.10: Maximum Principal Stresses for FGM model at x = -8.7mm, y = 4.6 mm

2.8 TRANSIENT ANALYSIS

After analyzing the results of steady state analysis; model 3, which has thinner Zirconia layer is chosen for transient analysis/thermal shock study. In steady state analysis, this model gives least thermal stresses.

To simulate thermal shock, a sudden thermal loading condition is modeled using transient analysis method. Analogues to equivalent streams of physics, a shock behavior is defined as sudden change in the input loading causing sharp change in output variables reaching them to the values which are higher than steady state values. Most of the times, the component failure is due to such sudden sharp loadings. As discussed in the problem statement, a feasible test case is designed to understand the shock behavior for FGM heat exchanger model.

Lots of research has been involved in the field of thermal shock behavior of FGMs. Zhao et al [22] worked on the theoretical analysis of transient thermo-mechanical behavior of FGM. For that they used a solid cylinder under the convective boundary condition. They also studied the effects of thermal shock on thermo-physical properties of FGM and a comparison with homogeneous materials. The numerical formulation for such thermal shock analysis was derived using separation of variables and displacement method technique.

As thermal loading conditions for each model vary from each other, the shock phenomenon becomes model specific. In our heat exchanger model, the complexity is

added by cold fluid internal channels passing through different layers of FGM. These channels, being on the interface of two different layers generate the distinct thermal stress values on each surface.

2.9 FINITE ELEMENT MODEL

The model meshed for steady state CFD analysis is used for transient analysis. Water channels are model using 3D Flotran fluid elements. Whereas, the body of heat exchanger is modeled with solid 3D Flotran elements. The physics applied to the model is modified so as to simulate stagnant water condition. A transient CFD analysis is then done over the model while results are written in output file at each time step.

As no cooling is imposed on the model; the heat flux, at the bottom surface of exchanger start heating up the whole unit. The stagnant water present in the channels also starts heating up. The limiting time step, before we start the cold water flow, is determined by the boiling point of water. The body is allowed to get heated until the temperature at bottom channels reach about 100° C.

After performing transient CFD analysis with stagnant water it is found that the water could remain stagnant until 15 sec. of heat flux input. In other words it takes around 15 sec. to heat up bottom channels up to around 100° C. After T = 15 sec. Fresh water starts entering channels with velocity of 0.5 m/s. The transient analysis is then further extended with monitoring the temperature change in the model for a finite time interval. Again, the temperature results are written out at each second.

In the 2nd step, the CFD model is converted into structural model. A steady state structural analysis is performed for each time step. The temperature loads on these models are applied from the results retrieved from each step of CFD analysis. With the maximum stress values achieved from each time step of structural analysis; a graph is plotted against time starting from 15 sec.

It is observed that the stresses start increasing rapidly after the cold water starts flowing through the channels. They reach their maximum value at T = 19 sec. and after that start decreasing. Slowly at around T = 26 sec. they approach the steady state values.

Figure 2.11 shows the principal stress contour of the model at T = 19 sec. You can see the stresses going high as 334 MPa, but still below the maximum allowable limit. Figure targets the specific point on the model, which is having the maximum stress value through out the transient case and shows the behavior of that point with respect to time. This point lies on rear bottom left corner of the lower layer channels.

It's observed (Figure 2.12) that due to sudden cooling there is a rise in stresses along the body of heat exchanger (time T=19 sec. to T=24 sec.). And with further time these stresses gradually lower down and reach steady state stress values (T = 26 sec.). As this maximum stress value lies below the allowable limit, this model can be considered as safe for this type of transient case.

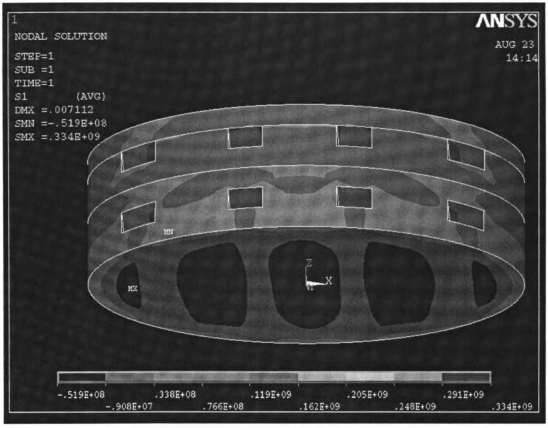

Figure 2.11: Maximum Principal Stress Contours at T = 19 sec.

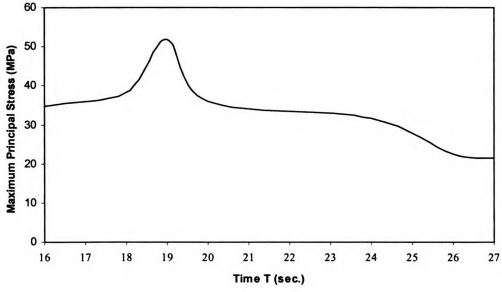

Figure 2.12: Maximum Principal Stress plot wrt time at (-7.88, -5.01, 1.33) co-ordinates

2.10 CONCLUSION

From the steady state analysis, it was proved that the variation in individual layer thickness in FGM plays an important role in minimizing stresses in the model. It was also proved that the model, which has thinner Zirconia layer, produces least stresses amongst the three models. Determining best of the models also depend upon applied clamping constraints. In all the cases we considered bottom surface clamping with ability to translate in x and y directions.

Transient state analysis results proved that the model can bear thermal shock and little delay over running cooling water over the channels could be allowed. For this analysis the thinner Zirconia layer model was chosen due to its high performance in steady state.

2.11 RECOMMENDATIONS FOR FUTURE WORK

Transient analysis can be further solved to tackle few more real life scenarios like variation in heat flux with respect to time, change in water temperature and velocity, change in convection coefficient and temperature of surrounding air with time etc. Care should be taken that in all of these cases temperature dependent material and water properties to be used.

Optimization of channel locations can be done so as to minimize stresses and increase cooling. Professional softwares like Ansys' Optimization Toolkit (using APDL) or HEEDS can be used for this purpose.

3. COUNTER FLOW HEAT EXCHANGER ANALYSES

3.1 INRODUCTION

Electronic cooling has been a research topic that has made possible the development of new generation of cooling hardware which has been focused in the area of thermal management. The upcoming electronic devices have heat dissipation increase in the order of magnitude. Mudawar [23] has explored the recent development of different cooling schemes in the area of high heat flux thermal management. Various schemes like pool boiling, detachable heat sinks, channel flow boiling, microchannel and mini-channel heat sinks were compared for efficiency. As discussed in the previous chapter, Functionally Gradient Materials (FGMs) prove to be efficient material in designing meso-scale heat exchangers where the thermal gradient loading conditions dominate stress values. This topic discusses the use of FGMs in fabricating a counter-flow heat exchanger and comparing the results with homogeneous materials for efficiency and durability.

The efficiency of heat exchanger is predicted by its Log Mean Temperature Difference (LMTD or ΔT_{lm}) value, as defined below:

$$\Delta T_{lm} = (\Delta T2 - \Delta T1) / [\ln(\Delta T2/\Delta T1)]$$

Where:

$\Delta T2$ = the larger temperature difference between the two fluid streams at either the entrance or the exit of heat exchanger

$\Delta T1$ = the smaller temperature difference between the two fluid streams at either the entrance or the exit of heat exchanger

LMTD is generally a representative of the temperature driving force for heat transfer in exchangers. The larger the LMTD, the faster heat transfers [24]. In counter flow heat exchanger, two fluids flow in opposite direction. Each of the two fluids enters the heat exchanger at opposite ends. As the cooler fluid exits heat exchanger where hot fluid enters heat exchanger, the cooler fluid will try to approach the inlet temperature of hot fluid. This makes counter flow heat exchanger most efficient (having maximum LMTD value) amongst the three popular types of heat exchangers (parallel, cross-flow and counter flow).

Using counter flow heat exchanger scheme also gives simplicity to the unit. No moving parts and compactness of the device can make is easy to maintain. Most of the times; the packaging material for electronics component is some combination of ceramics; mainly alumina. The heat exchanger which is required to carry out heat from those electronic component can also made of alumina or related composites. If such ceramics exchangers perform efficiently, a further effort can be made to combine heat exchanger and ceramic package together. This gives compactness to the whole system; the unit remains closer to heat source and thus the proposed heat exchanger becomes a multifunctional material

system. As discussed, multifunctionality comes from having the unit work as heat exchanger as well as being a packaging wall for whole electronic device. The meso-scale size of the unit helps in compaction.

Instead of using the heat exchanger model discussed in the previous chapter, we propose a new design for fluid channels. Designing fluid channel should be of greater interest in this study. Also, as in this heat exchanger model we have one hot fluid channel and another cold fluid channel separated by exchanger body, we experience thermal gradiency. To offset this thermal gradient effect we use FGM to fabricate the body of heat exchanger. Also we compare the stress results for FGM with homogeneous material to validate the efficiency of using FGM.

3.2 PROBLEM STATEMENT

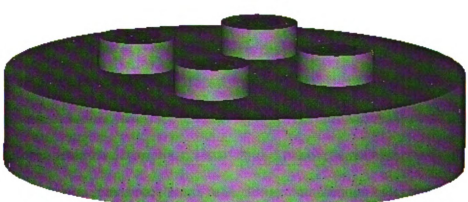

Figure 3.1: Proposed Heat Exchanger Model

Consider a counter-flow heat exchanger embedded in a meso-scale disk of homogenous material as shown in figure 3.1. This has two fluid channels, one on the top of another.

The four openings seen in the model are the inlets outlets of those channels. The two openings on horizontal orientation are the inlet and outlet for hot fluid channel and the two on vertical orientation are the inlet/outlet of cold fluid channel. Hot fluid flows through the channel located near bottom surface of the disc and cold fluid flows through the channel near top surface. A thermal gradiency exists in these kinds of models. The bottom surface remains at high temperature and the top one at low temperature. Thus for a homogenous material, bottom part expands more than the top one due to same CTE throughout the material. This induces thermal stresses in the body of heat exchanger disk.

The use of multi-layered ceramics (MLC) or FGMs (Functionally Gradient Material) is a perfect choice in this scenario. If from the bottom to top we use different layers of materials with distinct CTEs (Coefficient of Thermal Expansion), this thermal stress can be minimized.

Our objective is to compare this heat exchanger design using 6-layered FGM with homogenous material for thermal stresses and determine the effectiveness. Secondly, we need to optimize the design of heat exchanger for minimal stresses. If the use of FGM is proved to be efficient, we need to find out the best possible combination of different sets of FGM models (equal layered, unequal layered: thinner alumina layer and unequal layered-thicker alumina layer) by comparing the relative stress graphs. The 6-layered FGM decided to use in this problem is made of the combination of alumina and zirconia ceramics.

3.3 MODEL SETUP

The model setup process involves various design iterations. Optimized design for fluid channels evolve from design-analysis steps. The steps include performing CFD analysis on fluid channels varying channel dimensions and then suggesting a suitable design change based on the results.

3.3.1 DESIGN EVOLUTION

Design Evolution phase consisted of several design parameters. The geometry, location of channels, orientation of channels and determining maximum fluid velocity through the channels were few of the important ones.

CHANNEL DESIGN

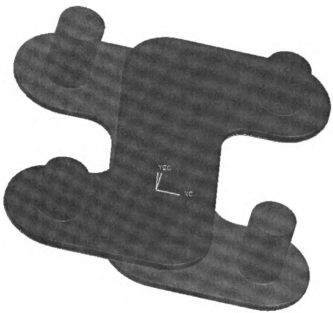

Figure 3.2: Initial Proposed Internal Channels

As seen in the figure the initial proposed channel shape contain 2 bends each at inlet and outlet. An adiabatic 3D CFD analysis is performed on these channels using FLOTRAN CFD module of *Ansys 7.0*. As fluid analysis requires different considerations, the mesh practice for CFD analysis changes substantially from that required for finite element analysis. In CFD, the mesh needs to be finer near channel boundaries as well as inlet and outlets. Thus the proper meshing guideline [25] is used for the analysis. Inlet velocity for the channel is specified as 0.5m/s and atmospheric pressure is assumed at outlet. The boundaries of channels are considered at zero velocity. To determine whether the flow is laminar or turbulent, Reynolds's number is calculated as follows [26]:

$$Re = \frac{\rho v_s L}{\mu} = \frac{v_s L}{\nu} = \frac{\text{Inertial forces}}{\text{Viscous forces}}$$

Where:

- v_s - mean fluid velocity,
- L - characteristic length (equal to diameter ($2r$) if a cross-section is circular),
- μ - (absolute) dynamic fluid viscosity, (1.002 cP for water)
- ν - kinematic fluid viscosity: $\nu = \mu / \rho$,
- ρ - fluid density. (1000 kg/m^3 for water)

By using above formula, with fluid velocity of 0.5 m/s, at the inlet with inlet diameter of 2.1 mm Reynolds number is 1050 (<2000) which makes the flow laminar. So a laminar flow CFD analysis is done.

After analyzing the results for above analysis, it is noticed that due to more bends and also smaller thickness of channels (0.15mm) solution do not converge for the velocity of 0.5 m/s. for this velocity it show that the fluid flow is reversed in direction. So, a similar analysis is repeated for reduced velocity values. It is seen that the allowable maximum velocity is very less (0.0001m/s) if the analysis has to converge. Such a slow velocity fluids could affect the performance of heat exchanger. A design change is suggested.

Thickness of channels is a fabrication constraint. Current manufacturing technique using fugitive phase to create these internal channels allow the maximum channel thickness not more than 0.15mm. So, the channel shape is optimized as shown in figure 3.3 to eliminate unnecessary bends and thus, the orientation of channels is also changed.

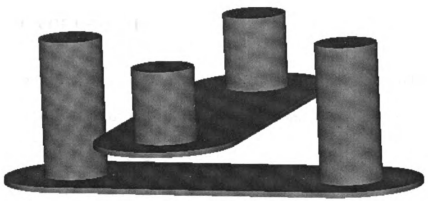

Figure 3.3: Refined channel design

CFD analysis is done with this new channel design keeping other analysis constraints same as in previous analysis. The results showed that for this design it is possible to force fluid with higher inlet velocity of 0.02 m/s without causing any fluid flow reversals (Figure 3.4).

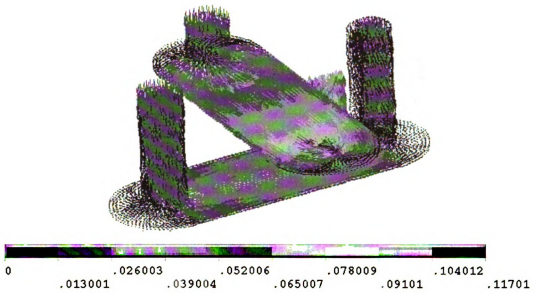

Figure 3.4: Vector Plot for Velocity profile in the channels

3.3.2 LOCATION OF CHANNELS

Next task in the design evolution is positioning channels in the heat exchanger body. Firstly a 6 equal layer FGM of Alumina and Zirconia combination is used to model heat exchanger body with channels (Figure 3.5). The channels are placed in such a way that the hot water channel is at the bottom of the disk, located near 100% Alumina layer (low Coefficient of Thermal Expansion material or CTE) and cold water channel near 100% Zirconia (high CTE). While seen from the top view, the hot water and cold water channels are oriented in perpendicular fashion to each other.

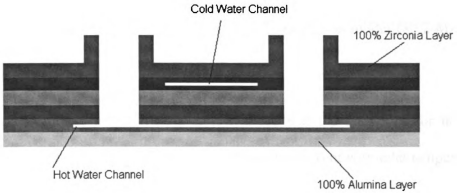

Figure 3.5: Section view of 6-layered FGM Heat Exchanger

The six equal layers in the FGM model are:

Layer 1: 100% alumina

Layer 2: 80% alumina + 20% zirconia

Layer 3: 60% alumina + 40% zirconia

Layer 4: 40% alumina + 60% zirconia

Layer 5: 20% alumina + 80% zirconia

Layer 6: 100% zirconia

A similar model is created using homogeneous material (as 100% alumina) to compare the results.

A multiphysics finite element analysis is done on both the models. For the initial CFD analysis the corresponding meshing strategies are implemented, while for the subsequent FEA model the solid mechanics meshing practices are followed. Hot water at 80° C is passed through the inlet channel. Cold water is 15° C at inlet. The disk outer surfaces are exposed to room temperature conditions.

The FEA results for the maximum principal stresses show that 6-layered FGM is in fact giving more stresses (667 MPa) as compared with homogenous model (80.2 MPa) (See figure 3.6 & 3.7).

Upon studying these surprising results it is realized that the inlet vent for hot water channel causes this high stresses. Water passes through this vent with inlet temperature as 80° C. As per the temperature contours, this inlet temperature remains constant throughout the vent. As vent passes across multilayer ceramic with gradually increasing CTE from bottom to top, each layer of ceramic expands differently with inlet temperature of 80° C. This causes thermal stress increase between the layers. So this model setup acts more like a combination of uniform thermal loading and thermal gradient loading thus fails to give excepted results with FGM model, which is designed in the favor of pure thermal gradient loading. Moreover as we look at the stress contours of homogeneous model, we see sudden stress rise from compressive to tensile values. Thus, these stresses can be minimized using more efficient channel design.

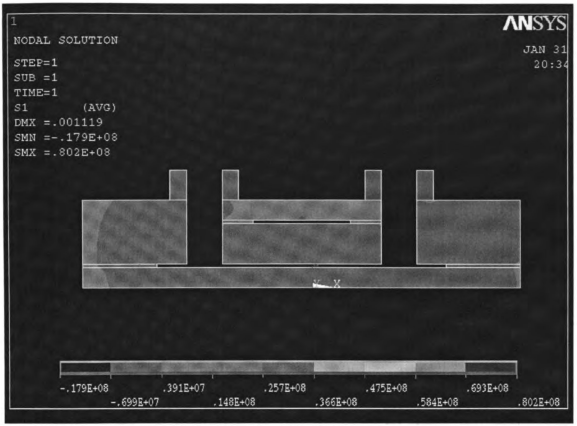

Figure 3.6: Section View: Maximum Principal Stresses: Homogenous Model

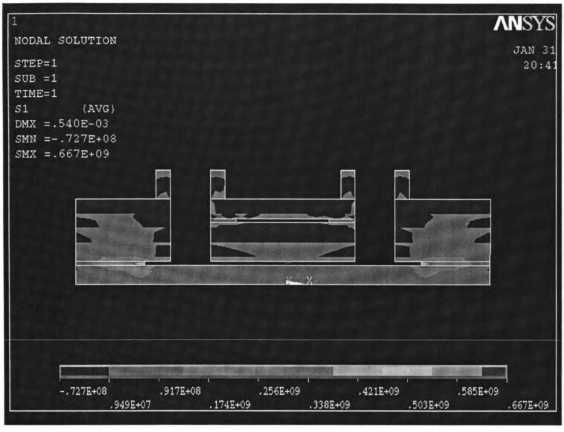

Figure 3.7: Section View: Maximum Principal Stresses: 6 Equal-layered FGM Model

3.3.3 NEW MODEL DESIGN

A new model design is proposed which will enable us to use the advantages of FGM and also improved the heat exchanger performance. The real need of FGM is in between hot water channel and cold water, as that area is undergoing a thermal gradient loading.

Inlet/outlet vent orientation of hot water channel is moved down, so that, it passes through only one layer of FGM (100% Alumina, bottom-most layer) and similarly, vents of cold water channels are moved up so that they pass only through 100% Zirconia layer. This orientation resolves the uniform thermal loading (causing high stresses) issue and

focuses more on thermal gradient loading issue, as now between hot and cold water channels there exists FGM to offset the thermal gradient.

The proposed new model also orients both the channels parallel to each other so as to achieve maximum heat transfer. Also the fluid flows are in opposite directions to set up a cross flow type heat exchanger (see figure 3.8).

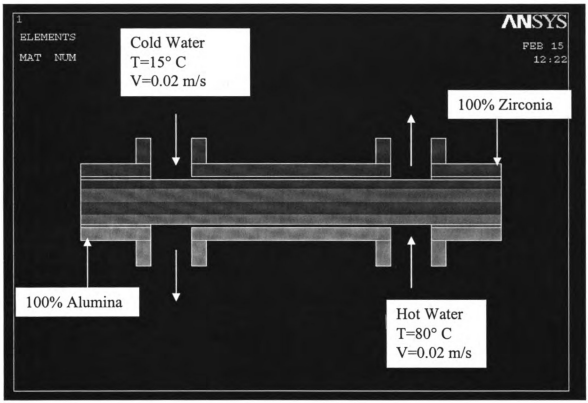

Figure 3.8: Section View: New Proposed Design: 6 equal-layer FGM

3.4 FINITE ELEMENT MODEL

The research is carried out by comparing the results of 6 equal layered FGM model with homogenous Alumina and Zirconia models. Later, FEA results of 3 different FGM models with different thickness layers are compared for maximum thermal stresses.

In the first step of the analysis a 3D thermal – CFD analysis is performed with various thermal loadings applied as shown in figure 3.8.

The solid, non channel area of the device is meshed with solid CFD elements. While meshing the channels, biased meshing approach is implemented. Mesh density is increased near boundaries. Fluid channels are very thin (0.15mm) compared to the overall size of model (18mm diameter X 3.6 mm thickness). Also 8 node 3D hexahedral elements are preferred for CFD analysis. So, while carrying out CFD analysis, channels are meshed with finer size elements and mesh density is increased at the solid layers near fluid channels. Care also to be taken for not exceeding maximum elements limit over the software version. This limit being different on fluid and solid elements, care needs to be taken so that fluid model element size is smaller than maximum number of solid model; as we perform weak coupled analysis, where we require converting fluid mesh into solid. Care also to be taken that all the 6 layers and channels are connected together with glue operation so as to maintain interlayer displacement continuity. Laminar flow is modeled as this model has low Reynolds Number (197) due to small hydraulic diameter and smaller velocity value.

3.5 RESULTS AND DISCUSSION

The equal layer FGM model is compared with homogenous models made of pure Alumina and pure Zirconia for the von mises stress values so as to see the efficiency of FGM model.

As shown in figure 3.9, FGM model gives lesser stress than pure Alumina model. Homogeneous model made of pure Zirconia produce the highest stress. Thus considering average stress distribution and stress concentration areas in these three different models, we conclude that the use of FGM proves to be the efficient choice in this application. Near the top surface of FGM model there is a little rise in stresses. For this reason we also study different thickness layer models so as to find which one gives minimal stresses.

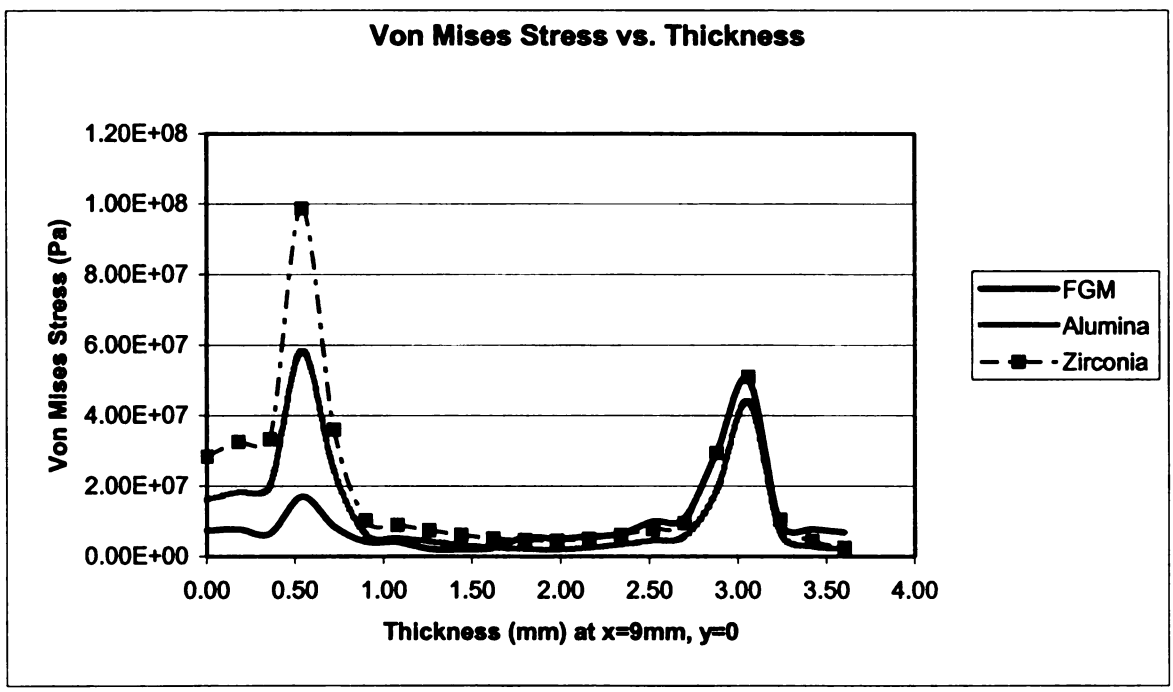

Figure 3.9: Von Mises stresses plot comparison for FGM and homogenous models

Figure 3.10 shows three different models of 6-layer FGM. Equal layer model has all the 6 layers of equal thickness, Model 1 (mentioned as 2 in fig.) has thinner alumina thickness at the bottom and thickness of layers gradually increase from bottom to top, from layers 2 to 5. Layer 1 and 6 are of same thickness in all the models so as to accommodate

inlet/outlet vents. Model 2 (mentioned as 3 in fig.) has thicker alumina at the bottom and thinner layers as we approach top.

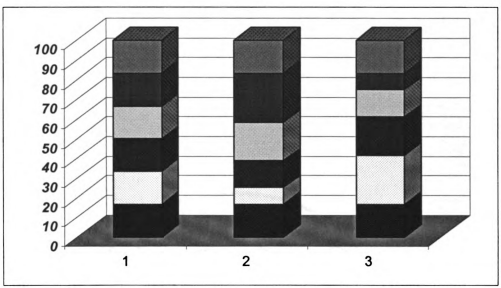

Figure 3.10: Three different types of FGM models (Equal thickness layers, Model 1, Model 2)

Figure 3.11 through 3.13 shows the maximum stress contours for Model 2 (thicker alumina) and Model 1 (thinner alumina) and equally thick layered model respectively. As far as the maximum stress values are concerned, model 2 (figure 3.11) gives minimal stresses (64 MPa) compared with Equal thickness (66 MPa) (figure 3.13) and Model 1 (93 MPa) (figure 3.12).

Figure 3.14 and 3.15 shows the graphic comparison between these three FGM models for maximum and minimum stress results respectively.

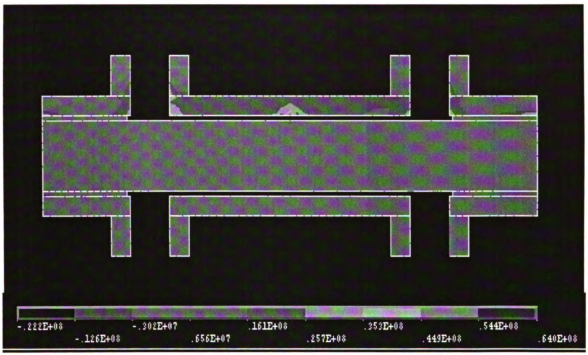

Figure 3.11: Max. Principal Stress Contour of Model 2 (thicker Alumina)

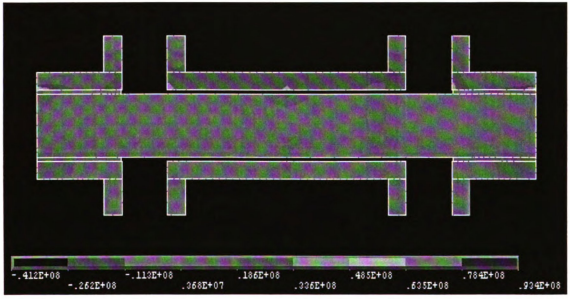

Figure 3.12: Max. Principal Stress Contour of Model 1 (thinner Alumina)

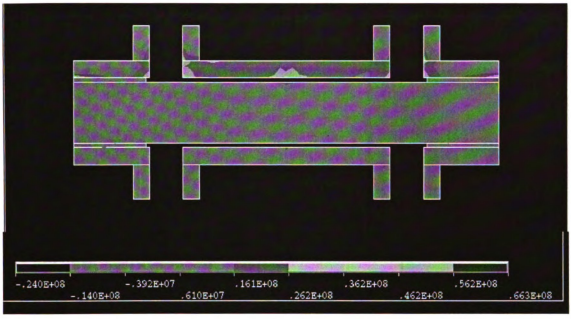

Figure 3.13: Max. Principal Stress Contour of Equally thick layer model

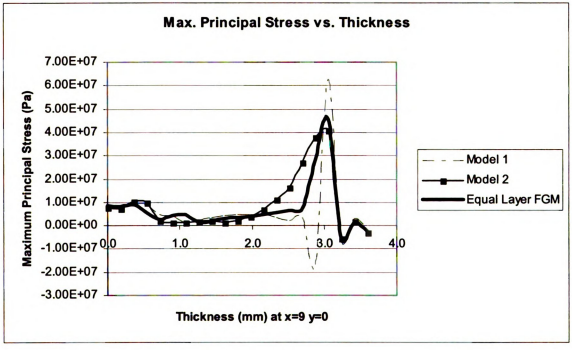

Figure 3.14: Max. Principal Stress Comparison for three FGM models

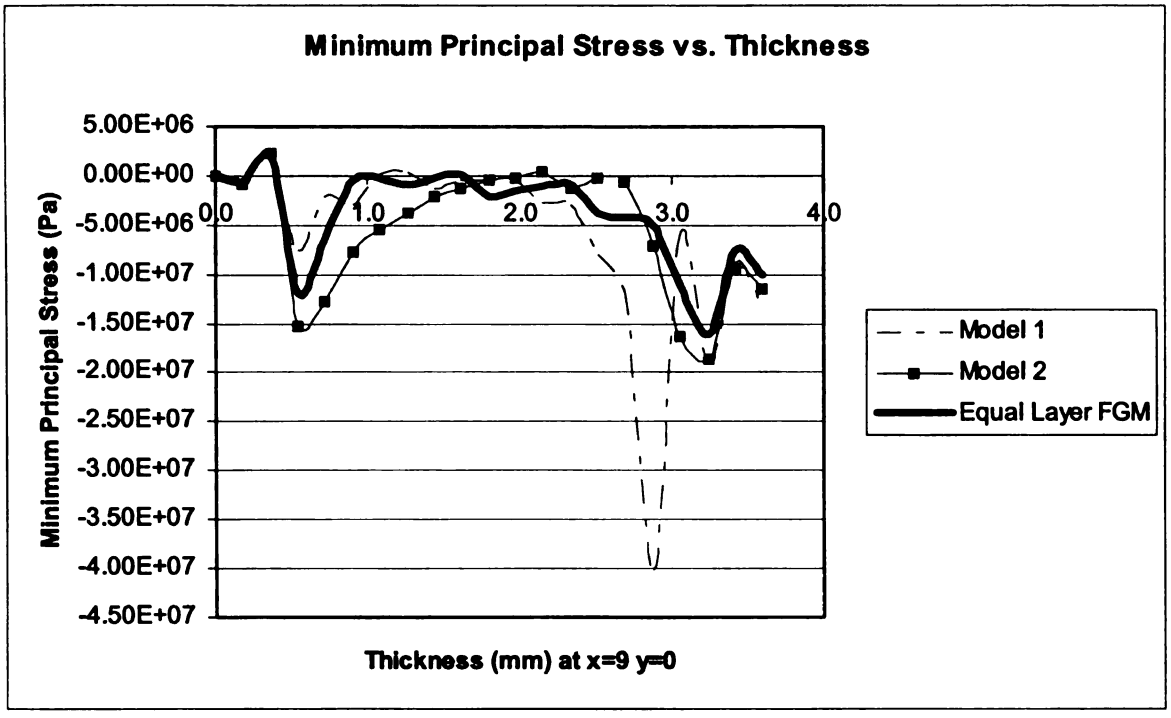

Figure 3.15: Min. Principal Stress Comparison for three FGM models

These graphs are plotted at the location where we see maximum/minimum stress results (or the location closer to the max/min stress areas) in all three models. From the above graphs it can be seen that model 1 (thinner Alumina) gives highest tensile as well as compressive stresses amongst the three models. Model 2 shows gradual change in stresses. Model 2 and Equal layer model show similarity in the stress values as we graduate from bottom to top. However as we approach top, equal layer model show higher maximum stress values while Model 2 shows lower minimum stress values. Considering minute difference in the values of equal thickness model and model 2 and considering the relative complexity in fabrications, equal thickness layer model can be recommended.

3.6 TEMPERATURE PROFILE

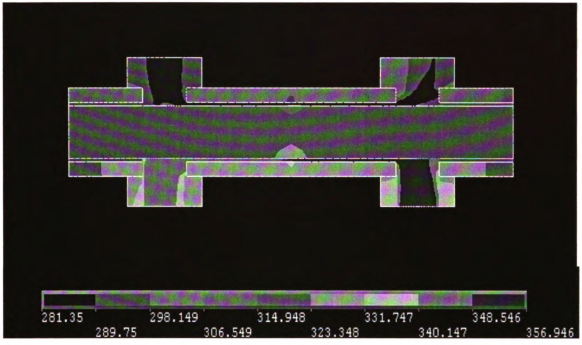

Figure 3.16: Section view of temperature contours (K) in Model 2

Even though our main interest is to minimize stresses in the model, as per the efficiency of heat exchanger is concerned we would be interested to compare temperature changes in the channels across different models. After looking through the temperature profiles at channels for all FGM and homogeneous models, it's observed that heat loss by hot fluid is maximum in the pure alumina model closely followed by the equal thickness layer model. Model 2 gives the least heat loss value. Since, the difference in these values is not much; we can conveniently consider similar efficiency across models.

3.7 CONCLUSION

The objective of this analysis was twofold. One, to understand the behavior of the heat exchanger for different type of channels, which will help us in optimizing the channel shape and location. Secondly, to compare the FGM model of heat exchanger with homogeneous models and compare the stress variations. Also to compare three different FGM models for understanding the stress change and recommending the best one in terms of stress values and stress contours.

From the numerical simulations, we finalized the channel shape which will eliminate uniform thermal loading. It is also seen that FGM model gives lesser stress values and more uniform stress contours. This is achieved by implementing the materials with gradual change in CTE to offset thermal gradient loading. So, the use of FGM is efficient in cross-flow heat exchanger model. We also compared three different FGM models. The model with thinner alumina layer (model 1) gave maximum stress values while model 2 (thicker alumina layer model) and equal thickness model gave similar stress results. In all the three FGM models, first and the sixth layer were of same thickness to avoid material change near inlet and outlet vents. Considering the efforts and accuracy required in modeling unequal layered model and similarity in the stress values, we recommend equally thick layered model for this particular application.

3.8 RECOMMENDATIONS FOR FUTURE WORK

Currently, the thickness of channels is constrained by its manufacturing process. In sintering of 6 layered FGM, a thin sheet of graphite in the shape of channels is kept between the ceramics at the locations where channels are designed. During sintering process, graphite evaporates and creates void area, which forms channels. Later inlet/outlet vents are drilled in the sintered body. As we increase the thickness of graphite sheet, the after sinter model develops cracks and warps near channel edges. This puts on the design constraint on the maximum allowed thickness of channels. Further process improvement can be suggested to increase channel thickness.

On the analysis front, a special transient case can be solved to measure thermal shock in the model. This can be achieved by considering no cold water flowing through the channels at the beginning of the cycle and hot water continues to flow. After a certain time frame cold water starts flowing through channels. A thermal shock is observed in this case. Some clamping constraints and outside temperature values can be changed to see its effect on the model.

APPENDIX A

Material properties of some common ceramics*:

	Materials	Alumina	Zirconia (Y_2O_3 stabilized)	Magnesia
Properties	Units			
Bulk Density	g/cm^3	3.85	6.0	2.5
Grain Size	μm	1-12	< 1.0	<20
Compressive Strength	MPa	2250	2000	190
Flexural Strength	MPa	400	800	85
Young's Modulus @ 20° C	GPa	385	200	250
Poisson's Ratio	-	0.22	0.23	0.18
Thermal Conductivity @ 20° C	W/m.K	28	2.9	32
Thermal Expansion Coefficient @ 20°C	10^{-6}/°C	7.9	9.5	13
Specific Heat	J/Kg.K	880	610	877

*Data collected from Morgan Advanced Ceramics Inc, Matweb, Martin Marietta Inc. etc.

APPENDIX B

Properties of the FGM (from Mori-Tanaka scheme)

Table I: Assuming Y-PSZ as the matrix phase and alumina as the particle phase

Y-PSZ Matrix (%)	Al_2O_3 Particle (%)	Young's Modulus (N/m²)	Poisson's Ratio	CTE (/°C)	Thermal conductivity (W/m/K)
100	0	2.00000E+11	0.3	1.03E-05	3
80	20	2.23300E+11	0.28767	9.78E-06	5.7018
60	40	2.49500E+11	0.27477	9.31E-06	8.6916
50	50	2.63684E+11	0.2682	9.08E-06	10.3106
40	60	2.78700E+11	0.2612	8.87E-06	12.022
20	80	3.11693E+11	0.24677	8.47E-06	15.7626
0	100	3.50000E+11	0.23	8.10E-06	20

Table II: Assuming alumina as the matrix phase and Y-PSZ as the particle phase

Y-PSZ Particle (%)	Al_2O_3 Matrix (%)	Young's Modulus (N/m²)	Poisson's Ratio	CTE (/°C)	Thermal conductivity (W/m/K)
100	0	2.00000E+11	0.3	1.03E-05	3
80	20	2.25000E+11	0.2865	9.75E-06	5.857
60	40	2.52120E+11	0.2729	9.27E-06	8.9491
50	50	2.66570E+11	0.2662	9.05E-06	10.5933
40	60	2.81640E+11	0.2593	8.84E-06	12.3091
20	80	3.13900E+11	0.2454	8.45E-06	15.9767
0	100	3.50000E+11	0.23	8.10E-06	20

Table III: Final averaged values

Y-PSZ (%)	Al_2O_3 (%)	Young's Modulus (N/m²)	Poisson's Ratio	CTE (/°C)	Thermal conductivity (W/m/K)
100	0	2.00000E+11	0.3	1.03E-05	3.00E+00
80	20	2.24150E+11	0.287085	9.77E-06	5.78E+00
60	40	2.50810E+11	0.273835	9.29E-06	8.82E+00
50	50	2.65127E+11	0.2672	9.07E-06	1.05E+01
40	60	2.80170E+11	0.26025	8.85E-06	1.22E+01
20	80	3.12796E+11	0.246085	8.46E-06	1.59E+01
0	100	3.50000E+11	0.23	8.10E-06	2.00E+01

REFERENCES

[1] Gehman, H. W., et al, "Columbia Accident Investigation Board," Report Volume 1, U. S. Government Printing Office, Washington, DC, August 2003.

[2] Mayeaux B.M.; Collins T.E.; Jerman G.A.; McDanels S.J.; Piascik R.S.; Russell R.W.; Shah S.R., "Materials Analysis: A Key to Unlocking the Mystery of the *Columbia* Tragedy", JOM, Volume 56, Number 2, 1 February 2004, pp. 20-30(11)

[3] Melis, M., Carney, K., Gabrys, J., Fasanella, E. and Lyle, K., "A Summary of the Space Shuttle Columbia Tragedy and the Use of LS- DYNA in the Accident Investigation and Return to Flight Efforts", 8th International LS-DYNA Users Conference, Dearborn MI, (2004).

[4] NSTS Shuttle Reference Manual (1988), Chapter 12: Space Shuttle orbiter Systems.

[5] Blosser M. L., "Development of Metallic Thermal Protection Systems for Reusable Launch Vehicle", NASA Technical Memorandum 1996.

[6] Chapter 3, "Contact Technology Guide", *Ansys* Release 9.0 Documentation.

[7] Souder B., "Fabrication of Core/Skin Unit for Perspirable Skin", Manufacturing Lab, Michigan State University, 2005/2006, Unpublished data.

[8] Case, E. Fei, R. Kwon, P., C. Kok Klenow B. and Rachedi, R., 2004, "Machining and Ceramic/ceramic Joining to Form Internal Meso-scale Channels," International Journal of Applied Ceramic Technology, 1, 1, pp. 95-103.

[9] Kok, C.K. and Kwon, P, 2004, "Compaction Models for Ceramic Powder in Making Meso-Scale Heat Exchangers," Transactions of NAMRII/SME, v. XXXII.

[10] Kwon, P. Kok, C. K., Fickes, D., Somerton, C. W., Shin H. W., .and Case, E. D., 2002, "Processing Issues in Fabricating Ceramic Micro-Heat Exchangers by Joining Components," Transactions of the American Ceramic Society, Westerville, OH.

[11] J. A. Davis, R. Venkatesan, A. Kaloyeros, M. Beylansky,S. J. Souri, K. Banerjee, K.C. Saraswat, A. Rahman, R. Reif, and J.D. Meindl, "Interconnect limits on gigascale integration (GSI) in the 21st century," Proceedings of the IEEE, vol. 89, no. 3, pp. 305-324, Mar. 2001.

[12] D. Gerlach and Y. Joshi, Parametric Thermal Modeling of 3D Stacked Chip Electronics with Interleaved Solid Heat Spreaders, Proceedings of ITHERM 2006, May 30-June 2, 2006, San Diego, CA.

[13] R.J. Phillips, "Microchannel Heat Sinks," In *Advances in Thermal Modeling of Electronic Components and Systems,* Edtied by A. Bar-Cohen and A.D. Kraus, ASME, New York, Vol. 2, 1990, pp. 109-184.

[14] Y. Joo, K. Dieu, and C. J. Kim, "Fabrication of Monolithic Microchannels for IC Chip Cooling", IEEE Micro Electro Mechanical Systems Workshop, Amsterdam, The Netherlands, Jan.-Feb. 1995, pp. 362-367.

[15] Weiping Liu and J. N. DuPont, "Fabrication of functionally graded TiC/Ti composites by Laser Engineered Net Shaping", Scripta Materialia, Volume 48, Issue 9, , May 2003, Pages 1337-1342.

[16] R. Watanabe, A. Kawasaki, "Development of Functionally Gradient Materials via Powder Metallurgy", Journal of the Japan Society of Powder and Powder Metallurgy (Japan). Vol. 39, no. 4, pp. 279-286. Apr. 1992.

[17] A. Neubrand, J. Rodel, "Gradient materials: an overview of a novel concept", Zeitschrift fur Metallkunde (Germany). Vol. 88, no. 5, pp. 358-371. May 1997

[18] T. Franklin, P. Kwon, "A Novel Processing Technique to minimize the residual stress- induced camber in fabricating Multi-Layered Ceramics and FGMs", unpublished data.

[19] Mori, T., and Tanaka, K., 1973, "Average Stress in Matrix and Average Elastic Energy of Materials with Misfitting Inclusions," Acta Metallurgica et Materialia, Vol. 21, pp. 571-574.

[20] Subramanian R., 2004, "Finite Element Analysis of a Functionally Gradient Meso-Scale Heat Exchanger", Chapter 3, Master Thesis Research, Michigan State University, Pages 36-41.

[21] *Ansys Theory Reference*, Chapter 11: Coupling.

[22] Zhao J., Ai X., Li Y, Zhou Y., "Thermal shock resistance of functionally gradient solid cylinders", Materials science & engineering: A, 2006, vol. 418, n°1-2, pp. 99-110.

[23] Mudawar, I., "Assessment of high-heat-flux thermal management schemes", IEEE transactions on components and packaging technologies, vol. 24, no. 2, June 2001, pp. 122-141.

[24] DOE-HDBK – 1012/1-92 June 1992, Thermodynamics, Heat Transfer and Fluid Flow.

[25] Goehner, U; Mauch, H, "FLOTRAN: Numerical method and industrial applications", INT J COMPUT APPL TECHNOL. Vol. 11, no. 3-5, pp. 199-202. 1998

[26] Fouz, Infaz "Fluid Mechanics," Mechanical Engineering Dept., University of Oxford, 2001, pp96